RECONSTRUCTING THE YIELD CURVE

Yan Liu
Jing Cynthia Wu

Reconstructing the Yield Curve
Yan Liu and Jing Cynthia Wu
NBER Working Paper No. 27266
May 2020
JEL No. E43

ABSTRACT

The constant-maturity zero-coupon Treasury yield curve is one of the most studied datasets. We construct a new dataset using a non-parametric kernel-smoothing method with a novel adaptive bandwidth specifically designed to fit the Treasury yield curve. Our curve is globally smooth while still capturing important local variation. Economically, we show that applying our data leads to different conclusions from using the leading alternative data of Gurkaynak et al. (2007) (GSW) when we repeat two popular studies of Cochrane and Piazzesi (2005) and Giglio and Kelly (2018). Statistically, we show our dataset preserves information in the raw data and has much smaller pricing errors than GSW. Our new yield curve is maintained and updated online, complemented by bandwidths that summarize information content in the raw data: https://sites.google.com/view/jingcynthiawu/yield-data.

Yan Liu
Purdue University
West Lafayette, IN 47906
liu2746@purdue.edu

Jing Cynthia Wu
Department of Economics
3060 Jenkins Nanovic Hall
University of Notre Dame
Notre Dame, IN 46556
and NBER
cynthia.wu@nd.edu

1 Introduction

Constant maturity zero coupon Treasury yields are a critical ingredient for researchers in macroeconomics and finance for studying the term structure of interest rates (e.g., Ang and Piazzesi (2003), Duffee (2002), Hamilton and Wu (2012), Diebold and Rudebusch (2013), and Wu and Xia (2016)), estimating return forecasting regressions (e.g., Fama (1984) and Cochrane and Piazzesi (2005)), analyzing monetary policy (e.g., Rudebusch (2002) and Bernanke and Reinhart (2004)), and pricing other assets and derivatives (e.g., Hull and White (1990), Jarrow and Yildirim (2003), Koijen et al. (2017) and Cieslak and Pang (2020)). We construct a new set of zero coupon yields that better represent information in the raw data. We make it available to researchers and will update it regularly: https://sites.google.com/view/jingcynthiawu/yield-data.[2]

The most popular zero-coupon Treasury yield curve datasets are Fama and Bliss (1987) and Gürkaynak et al. (2007) (GSW hereafter). However, both have their limitations. Fama and Bliss (1987) data have limited maturities (1, 2, $\cdots$, 5 years) and are only available at a monthly frequency.[3] Moreover, their yield curve is unsmoothed, and extending their data to more densely distributed and longer maturities could lead to large fluctuations in forward rates.[4] GSW discard all underlying securities with less than three months to maturity and all Treasury bills. Therefore, by construction, the short end of their yield curve is extrapolated and has large pricing errors. An imprecise short end has important consequences for medium- and long-term maturities because it prices coupons. Moreover, their parametric method, which focuses on fitting the medium term, also makes the long end of their yield curve subject to extrapolation errors. Despite these shortcomings, researchers heavily rely on the short and long ends of the GSW dataset because it is the only option with a wide range of maturities.

---

[2] The raw CUSIP-level coupon-bearing Treasury bond data come from the CRSP Treasuries Time Series.

[3] Their data are available from CRSP Treasuries.

[4] See Cochrane's (2015) comments on Joslin et al. (2014), which apply Fama and Bliss (1987) methodology to extend their data to more maturities.

To address these issues, we construct a new zero-coupon yield curve dataset with a kernel-smoothing method. Our dataset is at the daily frequency covering maturities of 1, 2,..., 360 months. We study its economic implications by revisiting the influential paper of Cochrane and Piazzesi (2005) (CP) for bond return-forecasting regression, and the recent work on excess volatility of long-term bond yields by Giglio and Kelly (2018) (GK).

For the CP return-forecasting regressions, using our data uncovers a robust loading pattern over five forward rates. The same pattern holds for bonds with different maturities and over different sample periods. This result is consistent with CP's main conclusion that one return-forecasting factor, which is a linear combination of forward rates, predicts excess returns. By contrast, estimates based on the GSW data do not permit a one-factor interpretation: the estimated loadings do not have a consistent pattern across maturity ranges or over time. Moreover, their loadings differ by an order of magnitude between CP's original sample period up to 2003, and the sample extended through 2019.

Next, we test the spanning hypothesis (whether the three yield factors are sufficient to predict bond returns) by regressing excess returns on the five principal components of the five forward rates. Using our yield curve, we find the fourth and fifth principal components have additional predictive power whether we base our conclusion on standard inference or the bootstrap procedure recently developed by Bauer and Hamilton (2018). This result is consistent with CP's conclusion as well as the literature that argues for unspanned factors (e.g., Duffee (2011)). By contrast, with GSW data, the higher-order principal components fail to show additional predictive power using CP's original sample period. Moreover, both the sign and the order of magnitude of the loadings change between CP's original sample period and the extended sample, indicating instability of the GSW yield curve.

For excess volatility, we calculate the variance-ratio statistic proposed by GK, which compares the unrestricted variance of the log price of a long bond with its variance imposing the no-arbitrage restriction. For 20-, 25-, and 30- year bonds, we replicate GK's variance ratios of 1.19, 1.38, and 1.62, respectively, using the GSW data. However, GK find larger

variance ratios (often above 2) across a variety of alternative asset classes. We show their smaller estimates for Treasury securities are likely driven by the GSW data. Using our data instead, the corresponding variance ratios become 1.62, 2.02, and 2.37, respectively, which is consistent with their overall conclusion, and strengthens their Treasury results.

What drives the different behaviors of our yield curve and GSW's? The main difference is that we use a non-parametric kernel-smoothing method based on Linton et al. (2001), whereas GSW apply Svensson's (1994) extension of Nelson and Siegel's (1987) parametric function. The non-parametric approach allows us to generate a globally smooth yield curve across maturities while still capturing important local variation.

We propose a novel approach to adaptively select bandwidths, which are the key to non-parametric methods. This procedure is specifically designed for the Treasury yield curve. The bandwidth is inversely related to the number of observed Treasury securities around a given maturity. The more data, the smaller the bandwidth. Conversely, parametric methods such as GSW have a fixed degree of freedom across all maturities. Our adaptive bandwidth selection allows us to keep securities at the end of the yield curve including Treasury bills, which we find contain important information in disciplining the overall behavior of the yield curve. In general, the flexibility of our non-parametric approach enables our dataset to represent information in the raw data, not only for the medium, but more importantly, for the short and the long run.

Our online zero-coupon yield curve data are complemented by a bandwidth file, which captures how much information is in the raw data. In general, the short term is associated with the smallest bandwidth, implying ample observations. By contrast, the bandwidth at maturities longer than 10 years is often large, due to intermittent issuance. Although a popular choice in the literature, the 30-year yield sometimes pools information from bonds with maturities that are 10 years away, even for the post-1990 sample. We recommend researchers use the bandwidth data as additional information to assess the quality of the zero-coupon yield curve and the availability of the raw coupon-bearing Treasury securities.

Another methodological contribution we make is to propose a sequential method to systematically delete outliers in the raw data as opposed to ad hoc methods that are often used in the literature. Our algorithmic approach is transparent and replicable for future research. Another benefit is that it helps us detect calendar-based anomalies. Specifically, we find the 1st, 15th, and last day of each month include an unusual number of outliers, whereas the days before and after these calendar days are much less noisy and display similar yield curves. The sequential method guarantees internal consistency of the yield curve across days. Interestingly, for monthly data, the most popular choices in the literature are the end of the month, the beginning of the month, and mid month. We show all of these choices are subject to a larger number of outliers. Instead, we recommend researchers use the second to last day of the month, the second day of the month, or the day before or after the 15th.

Having discussed how we construct the yield curve and its economic implications, we next probe into its statistical performance. We first compare our dataset with GSW in terms of how they fit the raw data in sample. We find that for maturities less than one year, GSW generate large and sometimes extreme pricing errors as high as 7% in annualized yield to maturity. Our method largely eliminates these extreme pricing errors and reduces the average pricing error by as much as 60%. GSW have large pricing errors in the short end because they choose not to use the raw data in that segment and subsequently extrapolate the short end from longer-term bonds. Note these large errors are not due to different outlier detection methods because we re-estimate their yield curves based on our filtered raw data for a fair comparison.

Our model also systematically outperforms GSW's for maturities longer than five years over the entire sample period, with a reduction of 39% in the average pricing error. This result highlights the extrapolation error in the long end of GSW's parametric curve. For the medium term, our model outperforms GSW's mainly during the low-interest-rate period after 2009. Overall, our model consistently outperforms GSW's across the entire maturity spectrum and over time.

4

The better in-sample performance of our yield curve is not an artifact of the more flexible non-parametric curve. The same comparison holds in an out-of-sample exercise: the average reduction in the out-of-sample pricing error is 49% across maturity buckets. Furthermore, we use the out-of-sample performance to determine the optimal bandwidths that best describe the Treasury data.

Our paper is organized as follows. In Section 2, we describe the non-parametric kernel-smoothing method. In Section 3, we discuss the adaptive bandwidth-selection procedure. Section 4 details our outlier detection algorithm and highlights a few Treasury pricing anomalies on selected days. Section 5 studies economic implications of our new data, and Section 6 focuses on its statistical performance. We offer concluding remarks in the final section.

2   Kernel-Smoothing Method

The goal is to extract a zero-coupon yield curve $y(n)$ for any maturity $n \in \mathcal{N}$ from observed Treasury bills, notes, and bonds, many of which have coupon payments. For theory, this section uses the support $\mathcal{N} = (-\infty, +\infty)$. In our application, we make it $\mathcal{N} = \{1, 2, ..., 360\}$ months.[5]

Estimation of the yield curve amounts to minimizing a weighted average of the distance between the fitted price and the observed price across all available bonds. The number of yields on the zero-coupon curve often exceeds the number of observations. To guarantee uniqueness and smoothness, one needs to impose additional constraints on the minimization problem. For example, Nelson and Siegel (1987) and Svensson (1994), which are the underlying methods GSW follow, assume a parametric functional form for the yield curve.

Alternatively, we rely on a non-parametric method. The main advantage of a non-parametric framework is that the yield curve does not need to have the same functional form across all maturities. Typically, the short end of the yield curve has more local patterns,

---

[5]For earlier years when relatively long-maturity bonds are not available, the support is $\mathcal{N} = \{1, 2, ..., n\}$, where $n < 360$ is the maturity limit that we will specify later on.

whereas longer-term yields are smoother. We design our non-parametric method with an adaptive bandwidth (in Section 3) to specifically target this feature of the yield curve. By contrast, parametric methods including the ones in the literature struggle to capture both features and need to make compromises.

Our framework builds on the work of Linton et al. (2001), who introduced a non-parametric kernel-smoothing approach in estimating the yield curve. In particular, the authors focus on the asymptotic distribution of the yield curve estimate when it is assumed to be locally linear.

Different from their paper, we focus on the empirical performance based on a finite sample of bonds. Specifically, our goal is to construct a smooth zero-coupon yield curve that best describes the raw data. We make the following methodological contributions. First, we propose a new method for bandwidth selection in Section 3 targeting the unique features of the Treasuries. Second, we provide yield estimates over a denser set of maturities compared to the literature, namely, $\mathcal{N} = \{1, 2, ..., 360\}$. Third, we derive analytical derivatives for the first-order conditions of the objective function to facilitate computation. Fourth, our objective function is weighted by durations of bonds, which follows the literature on fitting the yield curve parametrically and is new to the non-parametric literature.

2.1 Pricing Error for a Security

At a given point in time, suppose we focus on a generic bond.[6] It is characterized by its observed price p, its sequence of cash flows $\{c_j\}_{j=1}^{J}$ including its principal, and the corresponding maturities $\{\nu_j\}_{j=1}^{J}$. Given $y(\nu_j)$, the implied bond price $\widehat{p}$ is

$$\widehat{p} = \sum_{j=1}^{J} c_j \exp\Big(-y(\nu_j)\nu_j\Big). \tag{2.1}$$

The goal is to extract the entire zero-coupon yield curve $y(n)$ for $n \in \mathcal{N}$ from observed

---

[6]For brevity, we omit indicators for both time and bond for now.

bond prices. Note that $n \in \mathcal{N}$ denotes a maturity on the constant-maturity zero-coupon yield curve, whereas ν_j denotes the maturity of the cash flow c_j. $\{\nu_j\}_{j=1}^{J}$ do not cover the entire support $\mathcal{N}$, nor is ν_j necessarily in $\mathcal{N}$. Therefore, we cannot obtain $y(n)$ by simply inverting (2.1).

Instead, we connect a given ν_j with an arbitrary $n_j \in \mathcal{N}$ by approximating $y(\nu_j)$ with $y(n_j)$ using a first-order Taylor expansion:

$$y(\nu_j) \approx y(n_j) + (\nu_j - n_j)y'(n_j), \tag{2.2}$$

where $y'(n_j)$ is the first derivative of the yield curve evaluated at n_j. Now, we can approximate the bond price in (2.1) using (2.2)

$$\widehat{p}(n_1, n_2, ...n_J) \approx \sum_{j=1}^{J} c_j \exp\left[- \Big(y(n_j) + (\nu_j - n_j)y'(n_j)\Big)\nu_j\right], \tag{2.3}$$

where each $y(\nu_j)$ for the cash flow c_j is approximated by an arbitrary point on the zero-coupon yield curve $y(n_j)$.

In general, n_j could be any maturity in $\mathcal{N}$. However, the closer n_j is to ν_j, the more information the j-th coupon payment provides on $y(n_j)$. To capture this idea, we use a normal kernel-weighting function:

$$\begin{aligned} K(n_j, \nu_j) &= K_{h(\nu_j)}(n_j - \nu_j), \\ &= \frac{1}{\sqrt{2\pi h(\nu_j)^2}} \exp\left[- \frac{(n_j - \nu_j)^2}{2h(\nu_j)^2}\right], \end{aligned} \tag{2.4}$$

where $h(\nu_j)$ is the bandwidth parameter or the standard deviation of the normal distribution. The weighting function has two features. First, given the bandwidth, the weight is higher when n_j is closer to ν_j. Second, the bandwidth $h(\nu_j)$ is a function of ν_j. This is essential for our application and allows us to pool information more locally around one maturity and more globally around another.

When $h(\nu_j)$ goes to zero, the cash flow c_j only provides information for $y(\nu_j)$, but does not provide any information for $y(n_j)$ when $n_j \neq \nu_j$. Therefore, a narrow bandwidth overweights information locally and tends to generate a non-smooth yield curve. On the other hand, when $h(\nu_j)$ approaches infinity, all maturities are weighted equally. Hence, a wide bandwidth pools information more globally, but may generate yield curves that are overly smooth and lack local variation. We design our bandwidth to specifically target features of the Treasury yield curve; see details in Section 3.

Given the kernel weights, the kernel-weighted squared pricing error is

$$\mathcal{E} = \int \ldots \int (p - \widehat{p}(n_1, n_2, ...n_J))^2 \prod_{j=1}^J K(n_j, \nu_j) dn_j, \tag{2.5}$$

where $\widehat{p}(n_1, n_2, ...n_J)$ is defined in (2.3). Note we have $\int \ldots \int \prod_{j=1}^J K(n_j, \nu_j) dn_j = 1$, and $K(n_j, \nu_j)$ is positive everywhere, which makes it an appropriate density function.

Our choice of the normal kernel is motivated by two reasons. First, the fitting behavior is similar among different kernels, but the normal kernel has an advantage due to its analytical tractability (see, e.g., Wand and Jones (1994)). Second, in our framework, the continuous differentiability of the normal kernel allows us to derive the first-order conditions associated with (2.5) analytically, which greatly facilitates our estimation of a large dimensional yield curve (see Subsection A.1 for derivation).[7]

2.2 Summarizing Information across Bonds

We have thus far constructed the kernel-weighted squared pricing error for a generic bond. To combine information from all available bonds at a given point in time, we need to add up the squared pricing errors across bonds. Suppose I bonds are available on a given day. Let the kernel-weighted squared pricing error for bond i be $\mathcal{E}^i$ for $i = 1, \ldots, I$, where $\mathcal{E}^i$ is

---

[7]In contrast, alternative kernels such as the box kernel or the Epanechnikov kernel are not differentiable at the boundaries.

defined in (2.5).

The same discrepancy between the actual price and the fitted price has different implications for two bonds that have different maturity structures. For example, a \$1 pricing error is more pronounced for a short-term Treasury bill as opposed to a 10-year Treasury note. This difference can be captured by weighting $\mathcal{E}^i$ with $1/D_i^2$, where D_i is bond i's duration, defined as

$$D = \sum_{j=1}^{J} \frac{\nu_j c_j \exp(-\nu_j \bar{y})}{p},$$

and the yield to maturity (YTM) $\bar{y}$ is the constant discount rate that equates the present value of the bond's cash flows with its price:

$$p = \sum_{j=1}^{J} c_j \exp(-\nu_j \bar{y}). \tag{2.6}$$

The duration-weighted pricing error can be interpreted as the equally weighted error in the yield space. Therefore, our objective function is

$$\mathcal{S}(y(\cdot), y'(\cdot)) \;\; = \;\; \sum_{i=1}^{I} \frac{1}{D_i^2} \cdot \mathcal{E}^i, \tag{2.7}$$

where $y(\cdot)$ is the yield function and $y'(\cdot)$ is its first derivative. Our goal is to minimize this objective function to obtain $y(n)$ and $y'(n)$ for all $n \in \mathcal{N}$.

This weighting scheme is new in the non-parametric framework. We consider using durations to weight bond prices to be important, because doing so allows us to put more weight on fitting the shorter end of the yield curve, which affects coupon payments of bonds at all maturities. Several papers that estimate the yield curve parametrically have applied the same weighting scheme (e.g., Nelson and Siegel (1987), GSW).

Minimizing the objective function (2.7) with respect to $y(\cdot)$ and $y'(\cdot)$ is a non-trivial optimization problem. The main issue is that the integral in (2.5) does not have a closed-form

expression and needs to be approximated. Therefore, we need to choose a discrete support to facilitate computation. We choose $\mathcal{N} = \{1, 2, ..., 360\}$ months, which is denser than Jeffrey et al. (2006), for example. Our choice of a dense support in $\mathcal{N}$ requires estimating a large number of parameters. To alleviate some numerical burden, we derive analytical derivatives of the first-order conditions for (2.7), which provides efficient and accurate estimates of the yield curve; see Subsection A.1. Once we have estimates of the yield curve over this discrete support, our framework permits a kernel-weighted interpolation scheme to provide estimates for maturities that are not in the support. Our choice of a dense support ensures the estimated yield curve is smooth over the entire maturity range.[8] See details on estimation in Subsection A.1.

2.3 Model-Implied Bond Price

The model-implied bond price is

$$\widehat{p} = \int \ldots \int \widehat{p}(n_1, n_2, ...n_J) \prod_{j=1}^{J} K(n_j, \nu_j) dn_j. \tag{2.8}$$

Once we have the estimated $y(\cdot)$ and $y'(\cdot)$ over $\mathcal{N} = \{1, 2, ..., 360\}$, we approximate this object with (see our derivation in Subsection A.1)

$$\widehat{p} = \sum_{j=1}^{J} c_j \left(\frac{\sum_{n=1}^{360} K(n, \nu_j) \exp\left[-\left(y(n) + (\nu_j - n)y'(n) \right)\nu_j \right]}{\sum_{n=1}^{360} K(n, \nu_j)} \right). \tag{2.9}$$

In empirical sections, we compute $\widehat{p}$ using (2.9), and then calculate its associated yield to maturity.

---

[8]Note that interpolation guarantees the estimated yield curve is always continuous. However, a less dense support may lead to kinks in the estimated yield curve, which makes the yield curve less smooth.

3 Bandwidth

One main methodological contribution of our paper is to propose a bandwidth-selection method for the yield curve. The choice of bandwidth determines the smoothness of the estimated yield curve, which is crucial to generate a globally smooth yield curve while not missing important local variation. Section 3.1 proposes our adaptive bandwidth-selection procedure for the yield curve, and section 3.2 leverages the notion of bandwidth to summarize information content in the raw data.

3.1 Adaptive Bandwidth-Selection Procedure

We propose a data-driven approach for choosing bandwidths. We follow the basic idea of adaptive bandwidth selection in the literature on non-parametric estimators (see, e.g., Park and Marron (1990), Fan and Gijbels (1995), and Ruppert et al. (1995)). We are the first to apply an adaptive bandwidth-selection procedure to estimate the yield curve. Our specific choices are new to the literature.

For each ν that corresponds to a cash flow, we choose $h(\nu)$ such that N_0 bonds mature within the two-bandwidth interval around ν (i.e., $[\nu - 2h(\nu), \nu) \cup (\nu, \nu + 2h(\nu)]$). In our main analysis, we set N_0 at 8.[9] For a maturity segment with plenty of observations, the bandwidth $h(\nu)$ is small, and vice versa. To price this cash flow at ν, the relevant region in the zero-coupon yield curve is $n \in [\nu - 2h(\nu), \nu + 2h(\nu)]$, which covers 95% of probability weights.

In practice, observations are not equally spaced, and they are asymmetric around ν. For these reasons, we adapt our bandwidth-selection procedure as follows. Let $N([\nu_a, \nu_b])$ denote the number of bonds whose maturities fall into the interval $[\nu_a, \nu_b]$. We first define

---

[9]Our choice of $N_0 = 8$ is dictated by our out-of-sample forecasting results in Subsection B.5.

the left-hand-side bandwidth at maturity ν (i.e., $h^l(\nu)$) as

$$h^l(\nu) = \frac{1}{2}\min b$$
$$s.t. \quad N([\nu - b, \nu)) \geq N_0/2. \tag{3.1}$$

If no value of b satisfies $N([\nu - b, \nu)) \geq N_0/2$, we set $h^l(\nu)$ at $\nu/2$.

Similarly, define the right-hand-side bandwidth at maturity ν (i.e., $h^r(\nu)$) as

$$h^r(\nu) = \frac{1}{2}\min b$$
$$s.t. \quad N((\nu, \nu + b]) \geq N_0/2, \tag{3.2}$$

with $h^r(\nu) = \frac{1}{2}(n_{max} - \nu)$ if $N((\nu, \nu + b]) \geq N_0/2$ cannot be satisfied for any b, where n_{max} is the maximum maturity of the estimated yield curve.

Because the normal kernel is symmetric around ν, we consolidate $h^l(\nu)$ and $h^r(\nu)$ into one bandwidth:

$$h(\nu) \quad = \quad \min\{\max\{3, h^l(\nu), h^r(\nu)\}, 120\}, \tag{3.3}$$

where three months is the minimum and 120 months (i.e., 10 years) is the maximum bandwidth we set for any maturity.

Discussion Calculating $h^l(\nu)$ and $h^r(\nu)$ separately guarantees that we take information from both the left side and the right side of ν. This is important because the maturity distribution of outstanding Treasury securities on a given day often contains gaps, leading to asymmetry between $h^l(\nu)$ and $h^r(\nu)$; see Figure 1. For example, suppose a 10-year gap is present in the maturity space: no bonds exist with maturities between $\nu_a = 120$ (i.e., 10 years) and $\nu_b = 240$ (i.e., 20 years). Also suppose a large number of bonds exist with maturities that fall just below $\nu_a = 120$, implying $h^l(\nu_a)$ is small (in particular, $h^l(\nu_a) \ll$

12

Figure 1: **Outstanding Treasury Securities**
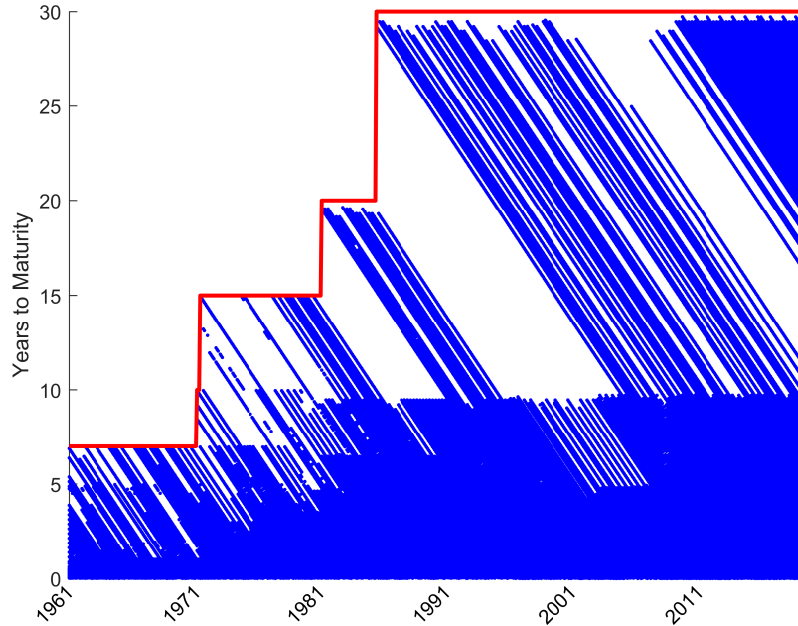
Notes: Maturity distribution of outstanding securities, 1961–2019.

$60 = \frac{1}{2} \times (240 - 120))$. Now consider the bandwidth choice at ν_a. If we set the bandwidth $h(\nu_a)$ at $h^l(\nu_a)$, the bond price at maturity ν_a only provides information for the yield curve up to maturity $\nu_a + 2h^l(\nu_a)$,[10] leaving the majority of the yield curve between ν_a and ν_b undetermined. Our solution is to set the bandwidth at $h^r(\nu_a)$, which is the larger one between $h^l(\nu_a)$ and $h^r(\nu_a)$.

For shorter maturities, many observations contain potential micro-structure noise and liquidity issues. For a fixed $N_0 = 8$, the bandwidth of $\max\{h^l(\nu), h^r(\nu)\}$ tends to be small. For example, $\max\{h^l(\nu), h^r(\nu)\}$ is, on average, around 0.5 months at the maturity of three months. Such a small bandwidth tends to generate substantial local variation in the estimated yield curve, which may not reflect the underlying true yield curve. Therefore, our choice of a minimum bandwidth of three months allows us to pool information from matu-

---

[10]This is only approximately true, because the normal kernel assigns a non-zero weight to any maturity. However, it assigns relatively large weights to observations that are within two bandwidths.

rities that are within half a year of ν to smooth out the estimated yield curve.

On the other hand, too large a bandwidth may bias the yield curve estimate because the Taylor expansion in (2.2) can be inaccurate. We therefore set the maximum bandwidth at 120 months. This maximum bandwidth only applies to long maturities where the data are sparse and have large gaps in the maturity distribution.

Fixing the number of local observations at N_0 allows us to pool roughly the same amount of local information to estimate the yield curve at each maturity. Another benefit is that it automatically adjusts for the total number of Treasury securities available at each date. When more bonds exist (as in the later part of our sample), bandwidths in general shrink, which allows us to better capture the local variation in the yield curve. Lastly, our bandwidth choice is controlled by only one parameter N_0, which facilitates our out-of-sample forecasting exercise that chooses the optimal N_0 in Subsection 6.4.

3.2   Information Content in the Raw Data

In this section, we leverage the notion of bandwidth to summarize the information content in the raw data. Different from (3.3), which is the bandwidth for each cash flow ν, we are now interested in the information contained at each maturity n on the zero-coupon yield curve. We propose using

$$h(n) \;\; = \;\; \min\{h^l(n), h^r(n)\}, \tag{3.4}$$

where $h^l(n)$ and $h^r(n)$ are calculated using (3.1) and (3.2). Note that if b does not exist for (3.1), we set $h^l(n)$ at ∞. The same applies to $h^r(n)$.

Why do we take the minimum instead of the maximum? We use the previous example with a 10-year gap in the maturity space between 10 years and 20 years to illustrate. For the bond with $\nu = 120$, $h^l(\nu) \ll h^r(\nu)$. But it needs to provide information to maturities within the gap $n \in (120, 240)$. This explains the maximum in (3.3). For $n = 120$ on the

14

Figure 2: **Bandwidth on Selected Dates**
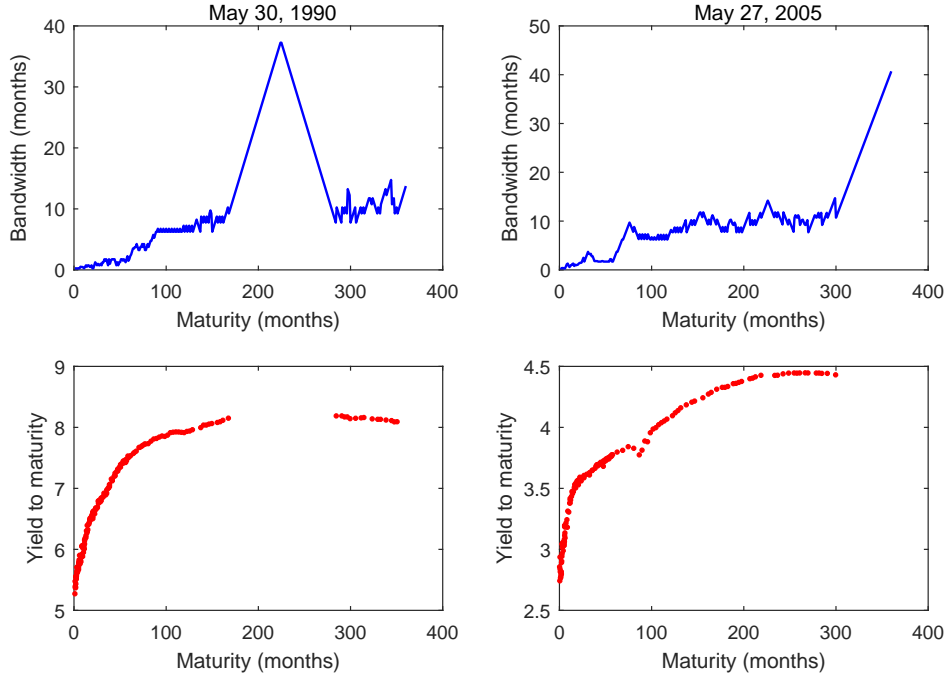
Notes: We plot the cross section of bandwidth for May 30, 1990, and May 27, 2005. The top panels plot the bandwidth. The bottom panels plot the yield to maturity.

estimated constant-maturity zero-coupon yield curve, we still have $h^l(n) \ll h^r(n)$. However, the information we use to estimate the yield at $n = 120$ primarily comes from bonds on the left side, and $h^l(n)$ is small. Hence, we need to take the minimum instead.

Figure 2 provides two examples. The left panel is May 30, 1990, and the right panel is May 27, 2005. We plot bandwidths at the top. Yield to maturity is at the bottom and each dot corresponds to one outstanding security.[11]

For both dates, the bandwidth increases with maturity in general, indicating observations are more concentrated on the short end. For May 30, 1990, no outstanding securities have maturities between 180 and 296 months, which results in the spike in bandwidth. On May 27, 2005, the longest maturity is 300 months, and we see the bandwidth increases sharply after that time.

---

[11]See Subsection 4.1 for details on the data.

Figure 3: **Time Series of Bandwidth**
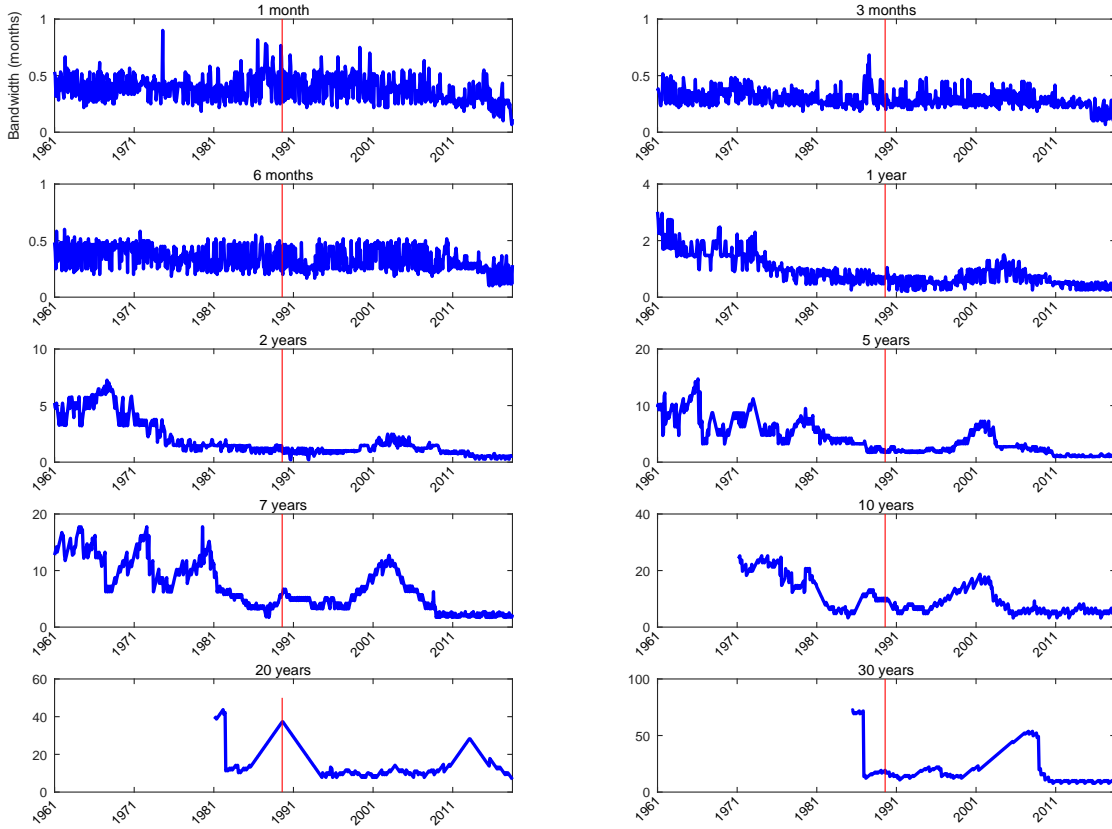
Notes: We plot the time series of bandwidth over the entire sample for 1961 to 2019, and the red vertical bar marks the beginning of 1990.

Figure 3 shows the time series of the bandwidth for various maturities, with the red vertical bar indicating the beginning of 1990. Data on the short end are abundant, and the bandwidths for one, three, and six months are generally below 0.5 months.

The Treasury does not always issue notes and bonds with longer maturities. For example, it started issuing the 10-year notes in September 1971, 15-year bonds in December 1971, 20-year bonds in July 1981, and 30-year bonds in November 1985. Even after these starting dates, they still issue them intermittently. This is consistent with Figure 1.

In general, the bandwidths become smaller after 1990 for maturities longer than one year. But they remain large for maturities longer than 10 years. The 30-year yield is popular for

studying the long end of the yield curve in the literature. However, due to the intermittent issuance, even the post-1990 sample's bandwidth can get as large as 60 months, implying a lack of observations and hence pulling information from bonds that are 10 years away. [12]

4 Raw Data and Outliers

4.1 Raw Data

The raw CUSIP-level coupon-bearing Treasury bond data come from the CRSP Treasuries Time Series. For each bond, we observe the end-of-day bid and ask (and average) prices, maturity, coupon payments, and schedule, as well as other characteristics. The sample is from June 1961 to December 2019 at the daily frequency.

Figure 1 summarizes the maturity structure for all outstanding Treasury securities over the entire sample period at the monthly frequency. The Treasury started issuing the 10-year notes in September 1971, 15-year bonds in December 1971, 20-year bonds in July 1981, and 30-year bonds in November 1985. We set the maximum maturity n_{max} accordingly, which is marked in red in Figure 1.

4.2 Outliers

In the literature on constructing a constant-maturity zero-coupon yield curve, outliers are usually deleted in an ad-hoc fashion.[13] We differ from the literature by taking a more systematic approach. We show our approach has important consequences in detecting periodic outliers that repeatedly appear on certain days of the month; see Subsection 4.3. Moreover, the nature of our approach makes it replicable for future research.

Note that our outlier detection does not drive the performance difference between our

---

[12]Note here we plot the bandwidth definition in (3.4) to summarize information content in the raw data, and we do not impose a lower bound and upper bound as in (3.3).

[13]For example, GSW state in Section 4, item (vi), "Other issues that we judgmentally exclude on an ad hoc basis."

yield curves and GSW's, as we later document in Section 6. That is because we re-estimate GSW's yield curves based on the same filtered data, which facilitates a fair comparison.

Specifically, we take a three-step approach to drop outliers or inappropriate data from the perspective of fitting the yield curve. The first two steps are similar to the literature and ensure our estimation contains only plain vanilla bonds not severely affected by liquidity issues. The last step is our novel algorithmic detection procedure, which systematically deletes outliers.

The three steps are described as follows:

I. *Only include fully taxable, non-callable, and non-flower bond issues (i.e., CRSP ITYPE equals 1, 2, 3, or 4).*

   This step ensures our sample does not include bonds with tax benefits and option-like features. Fama and Bliss (1987) apply the same filter.

II. *Exclude the two most recently issued securities with maturities of 2, 3, 4, 5, 7, 10, 20, and 30 years for securities issued in 1980 or later.*

   This procedure follows GSW and aims to delete on-the-run (or first "off-the-run") issues that often trade at a premium compared to other issues due to their liquidity and specialness.

III. *Sequentially delete outliers based on the fitted yield curve from the day before, where statistical cutoffs are computed using a segment of maturities.*

   This step is new. Our approach is algorithmic in nature (as opposed to the ad-hoc procedures in the literature), which makes it replicable in future research.[14]

Steps I and II of our filtering procedure are similar to Fama and Bliss (1987) and GSW. The main difference from GSW is that we do not discard securities with shorter maturities

---

[14]There is no escaping that any outlier detection algorithm has some subjective element to it. GSW exclude outliers on an ad hoc basis. Fama and Bliss (1987) drop observations when forward rate reversal exceeds a pre-specified threshold level.

or Treasury bills. We argued in Subsection 3.2 that these securities contain important information, and in Section 6, we subsequently show the importance of keeping them.

Three important features mark Step III of our filtering procedure. First, we adaptively drop outliers using information from the previous day. This approach helps ensure internal consistency of the yield curve across days. Second, we compute summary statistics by maturity segments, and use them to determine outliers within each segment. This takes into account the differences in data quality across the maturity spectrum. Lastly, our statistical cutoffs adjust for time-varying data quality, allowing us to keep bond observations that are likely affected by microstructure noise during market stress or illiquidity.[15] Our algorithm strikes a balance in dropping extreme observations and keeping information. We provide details in Subsection A.2.

4.3 Anomalies at the Beginning, Middle, and End of the Month

Our sequential approach for deleting outliers works particularly well when the amount of noise spikes drastically on certain calendar days, and allows us to detect abnormal observations. We find that the 1st, 15th, and last day of each month frequently display a peculiar amount of outliers.

The fist two columns of Figure 4 show two examples around the end of a month and the beginning of the next. The yield to maturity is relatively smooth on the second to last day of the month (the top row) and the second day of the next month (the bottom row) with a few outliers (marked by red "+"s). They also look similar to each other. By contrast, the last day of the month (the second row) is much noisier. The outliers are mainly concentrated at the short end of the curve up to about five years, and they partially extend to the first day of the next month (the third row) and disappear the next day (the bottom row).

The three panels on the right provide summary statistics. The distribution of the number

---

[15]While we maintain the same 3.0-IQR rule in our outlier detection (see Subsection A.2), IQR becomes larger during market stress, allowing us to keep more observations.

Figure 4: **Beginning- and End-of-the-Month Anomalies**
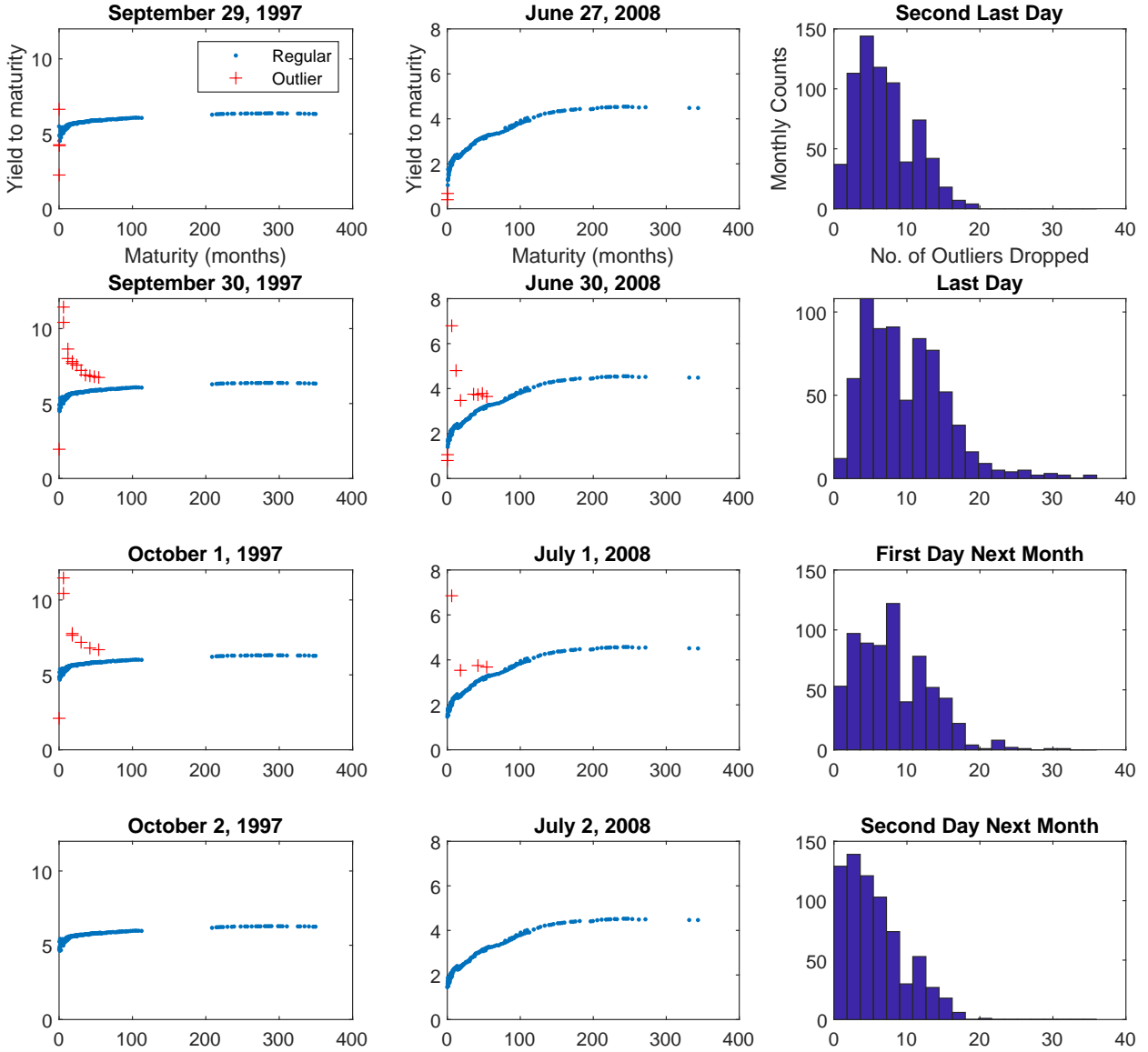
Notes: The first two columns plot the yield to maturity for September 29, 1997, to October 2, 1997 (first column) and June 27, 2008, to July 2, 2008 (second column). Red '+'s mark outliers and blue dots denote bonds we keep. The last column shows the distribution of the number of outliers, and the sample is from June 14, 1961, to December 31, 2019.

of outliers has a longer right tail for the last day of the month and the first day of the next month compared to their adjacent days. We find a similar anomaly for the 15th of the month; see details in Figure B.2 of Subsection B.2. We inspect these calendar-based anomalies and

20

find they are likely associated with the maturity calendar of Treasury notes and bonds, which are set to the 15th or end of the month, although the maturity calendar does not explain why end-of-month anomalies spill over to the beginning of the month.[16]

These anomalies have important implications for the choice of data. For monthly frequency, the most popular choices in the literature are the end of the month, the beginning of the month, and mid month. We have shown all of these choices are subject to a larger number of outliers. Instead, we recommend researchers use the second to last day of the month, the second day of the month, or the day before or after the 15th. For this reason, our analyses with monthly data and our online monthly yield curve data use the second to last day of the month to proxy for the end-of-the-month yield curve.

5   Economic Implications of the New Yield Curve

With our newly constructed zero-coupon yield curve, we revisit two prominent studies using the Treasury yield curve: the predictability of bond risk premia of Cochrane and Piazzesi (2005) (CP) and the excess volatility of long-term bond prices of Giglio and Kelly (2018) (GK). Note we focus on the comparison for the conclusion drawn based on our data with that based on GSW's data. For most of our analyses in Section 5 and Section 6, we do not compare with Fama and Bliss (1987)'s data because of their limited maturities (in total five maturities available from one to five years) and frequency (monthly only). The only exception is CP, where we present results using Fama and Bliss (1987) in Appendix B.1.

5.1   Cochrane-Piazzesi Return-Forecasting Regressions

CP's seminal paper finds that although three yield factors explain the majority of the cross-sectional variation of the yield curve, an additional return-forecasting factor, which is a linear combination of forward rates, predicts excess returns. This leads to a growing literature on

---

[16]See maturity calendar on TreasuryDirect: https://www.treasurydirect.gov/instit/annceresult/annceresult_query.htm.

the spanning hypothesis (whether the three yield factors are sufficient for predicting bond returns), which Duffee (2011) formalizes. For more references, see Cooper and Priestley (2009), Ludvigson and Ng (2009), Greenwood and Vayanos (2014), and Cieslak and Povala (2015).

We revisit CP's analysis and study the economic consequences of using different underlying zero-coupon yield curves. We first repeat CP's analysis using the same sample period and forward rates with the same maturities. Then, we extend along several dimensions.

First, we introduce some notation. Define the zero-coupon yield at t with a maturity of n as $y_t(n)$. The price of the n-year discount bond at time t relates to the zero-coupon yield as follows:

$$\log P_t(n) = -n y_t(n), \tag{5.1}$$

where n is maturity in years as in CP.

The forward rate with maturity n at time t is defined as the return for a loan starting at $t + n - 1$ and maturing at $t + n$:

$$f_t(n) = \log P_t(n - 1) - \log P_t(n). \tag{5.2}$$

The holding-period return of buying an n-period bond and selling it one year later is

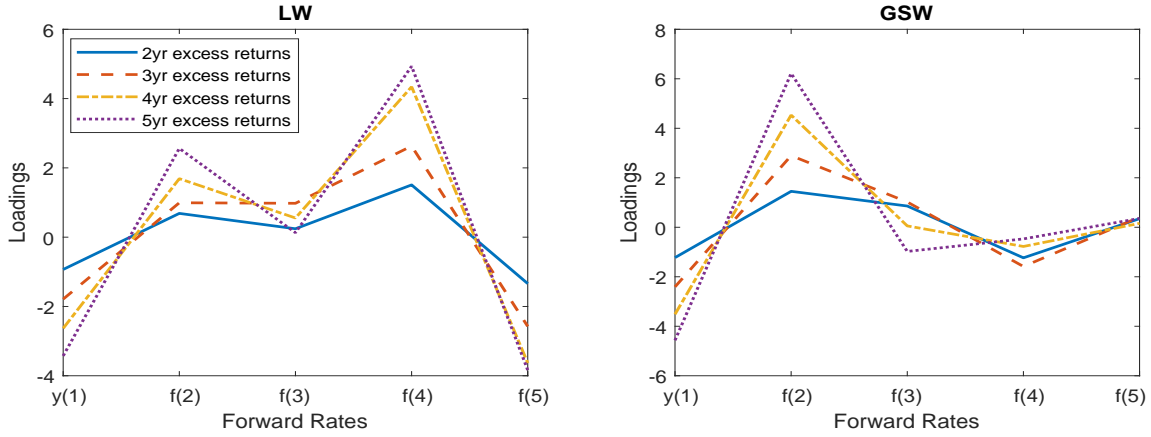$$r_{t+1}(n) = \log P_{t+1}(n - 1) - \log P_t(n). \tag{5.3}$$

The excess return is

$$rx_{t+1}(n) = r_{t+1}(n) - y_t(1), \tag{5.4}$$

where $y_t(1)$ is the one-year risk-free rate.

Figure 5: **CP Loadings of Individual Excess Returns**

Notes: X-axis: independent variables $y_t(1), f_t(2), ..., f_t(5)$. Different lines represent excess returns with different maturities $rx_{t+1}(2), ..., rx_{t+1}(5)$. We use CP's original sample from 1964-2003.

To repeat CP's analysis, we run the following return-forecasting regressions. The dependent variables are the excess returns of bonds with maturities of two to five years $rx_{t+1}(2), ..., rx_{t+1}(5)$. The independent variables are the forward rates: $y_t(1), f_t(2), ..., f_t(5)$. The regression has an intercept. The sample is CP's original: monthly from 1964 to 2003.

Figure 5 plots the loadings (regression-slope coefficients). Different lines represent maturities of excess returns (dependent variables) from two to five years. The X-axis denotes forward rates at different maturities (independent variables).

The left panel plots the loadings using our data. The five lines display the same "M" shape. CP highlight one single return-forecasting factor that predicts all excess returns. Although we do not have the tent shape as in CP, the same "M" shape across different maturities is consistent with CP's main conclusion of one return-forecasting factor.[17] By contrast, the patterns of loadings in the right panel using the GSW data are different across

---

[17]We replicate CP's tent shape in the left panel of Figure B.1 using Fama and Bliss (1987) data. The main driver between their tent shape and our M shape is multicollinearity: $f_t(2), f_t(3), f_t(4)$ are highly correlated with correlations between 0.97 and 0.98 in both ours and Fama and Bliss (1987)'s data. The fact that multicollinearity drives the tent shape away is also found by Hodrick and Tomunen (2018) in their international study. Moreover, it also changes the tent shape by simply extending the Fama and Bliss (1987) data (see the middle panel of Figure B.1). However, two main conclusions are consistent between Fama and Bliss (1987) and our data. First, both imply higher loadings for the three forward rates in the middle than for $y_t(1)$ and $f_t(5)$. More importantly, both have one single return-forecasting factor.

Figure 6: **CP Loadings of Average Excess Returns**
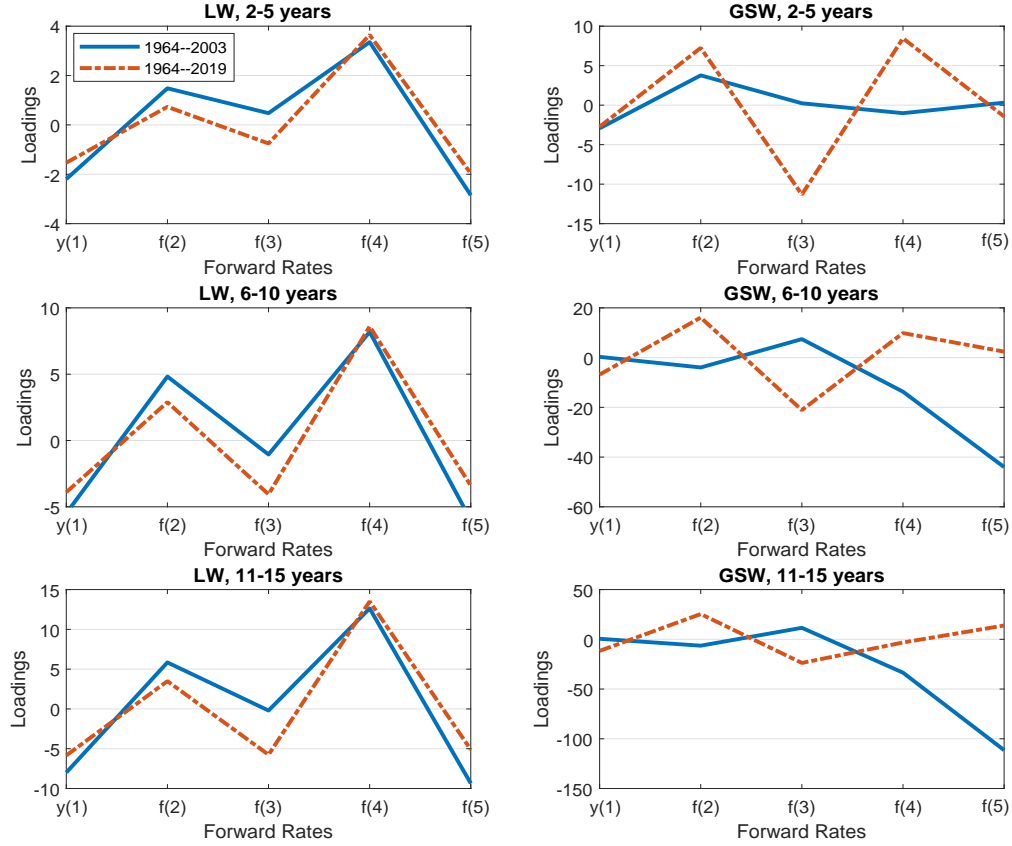
Notes: X-axis: independent variables one- to five-year forward rates $y_t(1), f_t(2), ..., f_t(5)$. Dependent variables are average excess returns. Bond maturities in the top panels are 2 to 5 years, 6 to 10 years in the middle panels, and 11 to 15 years in the bottom panels. Blue lines are CP's original sample from 1964-2003; red lines in the middle and bottom panels are the extended sample from 1964-2019.

maturities. In particular, the loading on $f_t(3)$ is higher than $f_t(4)$ for excess returns of two to four-year bonds. But this pattern is reversed for the five-year bond.

Next, we summarize results for the average excess returns $\overline{rx}_{t+1}^{(2\to5)} = \frac{1}{4}\sum_{n=2}^{5} rx_{t+1}(n)$. The blue lines in the top panels of Figure 6 take the average of the four lines in Figure 5 to compute the average loading between two and five years. We then extend the sample to current and plot the loadings for the 1964-2019 sample in the red dashed lines. We also extend the dependent variables to longer maturities, and plot loadings of 6- to 10-year bonds $\overline{rx}_{t+1}^{(6\to10)} = \frac{1}{5}\sum_{n=6}^{10} rx_{t+1}(n)$ in the middle panels, and 11- to 15-year bonds

$\overline{rx}_{t+1}^{(11\to15)} = \frac{1}{5}\sum_{n=11}^{15} rx_{t+1}(n)$ in the bottom panels.

The same "M" shape preserves remarkably well with our dataset in the left three panels, which implies one single return-forecasting factor prevails across different sample periods and maturities. That is not the case with GSW data. Among the six lines in the right panels, the shape changes over time and across maturities. For example, in the bottom-right panel, the loadings between the 1964–2003 sample and the 1964–2019 sample are negatively correlated. Moreover, the loadings differ by an order of magnitude between the two samples: the largest loading (in absolute value) is 25.4 for the 1964–2003 sample but increases to 111.4 for the 1964–2019 sample.

The left panel of Table 1 reports the loadings of regressing the average bond excess returns between two and five years on $y_t(1), f_t(2), ..., f_t(5)$. The loadings coincide with the top panels of Figure 6.

The return-forecasting regression has overlapping observations. To adjust for them, we make statistical inference using two alternative methods. First, we follow CP and calculate t-statistics and p-values using Newey-West standard errors with 18 lags. Second, we use the bootstrap procedure recently developed by Bauer and Hamilton (2018) (BH), and compute the 5% critical values based on the bootstrap distributions and the corresponding p-values.[18]

We note that besides $y_t(1)$ (the log one-year bond yield), the other forward rates are never significant with the GSW data. With our data, $f_t(4)$ and $f_t(5)$ are highly significant using both Newey-West and BH bootstrap-based p-values. This result is consistent with the stable "M" shape loadings on forward rates in Figures 5 and 6. Moreover, our R^2's are in the same ballpark as the ones using Fama and Bliss (1987) data (see Table B.1), whereas GSW produce smaller R^2's.

In the right panel of the Table 1, we conduct a test for the spanning hypothesis by regressing excess returns on the five principal components ($PC1$-$PC5$) of the five forward

---

[18]We focus on the bias-corrected bootstrap procedure recommended by BH. Small sample bias is a prevailing issue for modeling the yield curve because of its persistence. See Bauer et al. (2012, 2014) for further discussion.

Table 1: **CP Regression Results (Predicting 2- to 5-Year Bond Returns)**

LW Data

		Forward Rates					PCs					R-square
		$y(1)$	$f(2)$	$f(3)$	$f(4)$	$f(5)$	$PC1$	$PC2$	$PC3$	$PC4$	$PC5$	
(1964-2003)	Loadings	-2.194	1.483	0.476	3.353	-2.846	0.164	-1.533	-3.795	1.664	-2.651	0.303
	NW t-stat [NW p-value]	-4.597 [0.00]	1.359 [0.17]	0.294 [0.77]	2.483 [0.01]	-3.253 [0.00]	1.879 [0.06]	-4.519 [0.00]	-3.827 [0.00]	1.316 [0.19]	-1.340 [0.18]	
	BH 5% c.v. [BH p-value]	5.620 [0.15]	3.785 [0.65]	2.524 [0.82]	2.324 [0.04]	2.588 [0.01]	4.077 [0.41]	5.584 [0.13]	4.852 [0.16]	2.538 [0.32]	2.445 [0.29]	
	F-stat [p-value]									5.341 [0.01]		
	BH 5% c.v. [BH p-value]									4.483 [0.03]		
(1964-2019)	Loadings	-1.533	0.732	-0.752	3.646	-1.966	0.058	-1.316	-1.960	2.590	-2.886	0.217
	NW t-stat [NW p-value]	-3.110 [0.00]	0.744 [0.46]	-0.544 [0.59]	3.437 [0.00]	-2.350 [0.02]	0.984 [0.33]	-4.262 [0.00]	-2.092 [0.04]	2.408 [0.02]	-1.722 [0.09]	
	BH 5% c.v. [BH p-value]	5.199 [0.42]	3.149 [0.71]	2.420 [0.67]	2.124 [0.00]	2.294 [0.04]	3.604 [0.63]	5.712 [0.19]	4.183 [0.49]	2.260 [0.04]	2.299 [0.15]	
	F-stat [p-value]									13.266 [0.00]		
	BH 5% c.v. [BH p-value]									4.042 [0.00]		

GSW Data

		Forward Rates					PCs					R-square
		$y(1)$	$f(2)$	$f(3)$	$f(4)$	$f(5)$	$PC1$	$PC2$	$PC3$	$PC4$	$PC5$	
(1964-2003)	Loadings	-2.929	3.774	0.240	-1.016	0.319	0.154	-1.485	3.713	-2.818	-0.240	0.244
	NW t-stat [NW p-value]	-4.026 [0.00]	0.613 [0.54]	0.012 [0.99]	-0.039 [0.97]	0.027 [0.98]	1.575 [0.12]	-3.461 [0.00]	2.796 [0.01]	-0.631 [0.53]	-0.007 [0.99]	
	BH 5% c.v. [BH p-value]	4.039 [0.05]	2.358 [0.61]	2.138 [0.99]	2.132 [0.97]	2.156 [0.98]	3.831 [0.48]	5.853 [0.33]	3.595 [0.14]	2.113 [0.56]	2.119 [0.99]	
	F-stat [p-value]									0.658 [0.52]		
	BH 5% c.v. [BH p-value]									3.058 [0.52]		
(1964-2019)	Loadings	-2.728	7.248	-11.315	8.463	-1.434	0.055	-1.263	1.218	6.441	14.735	0.168
	NW t-stat [NW p-value]	-4.088 [0.00]	1.449 [0.15]	-0.721 [0.47]	0.430 [0.67]	-0.167 [0.87]	0.861 [0.39]	-3.501 [0.00]	1.187 [0.24]	1.965 [0.05]	0.549 [0.58]	
	BH 5% c.v. [BH p-value]	3.519 [0.02]	2.167 [0.19]	2.081 [0.51]	2.117 [0.69]	2.096 [0.88]	3.563 [0.68]	5.901 [0.38]	2.864 [0.40]	2.069 [0.06]	2.095 [0.61]	
	F-stat [p-value]									6.623 [0.00]		
	BH 5% c.v. [BH p-value]									3.042 [0.00]		

Notes: The dependent variable is the one-year excess return $\overline{rx}_{t+1}^{(2\to5)} = \frac{1}{4}\sum_{n=2}^{5} rx_{t+1}(n)$. The independent variables are the forward rates: $y_t(1), f_t(2), ..., f_t(5)$, or the five PCs ($PC1$-$PC5$) The regression has an intercept. NW t-stats and NW p-values are computed using Newey-West standard errors with 18 lags. F-stats and the associated p-values report the joint F test for $PC4$ and $PC5$. For both t stats and F stats, we also report the corresponding 5% critical values and p-values of the bootstrap distributions of Bauer and Hamilton (2018).

rates. The null hypothesis for the spanning hypothesis is that the loadings on $PC4$ and $PC5$ are jointly zero. We report the F-statistics and the associated p-values, as well as BH's 5% critical values based on the bootstrap distributions and the corresponding p-values.

Using our data, $PC4$ and $PC5$ are jointly significant in both sample periods with both standard and BH p-values. This result is consistent with CP's original conclusion as well as the literature that argues for unspanned factors; see, Duffee (2011).[19] By contrast, the GSW data fail to reject the null hypothesis for CP's original sample from 1964 to 2003, with both p-values at 0.52.

Furthermore, the loadings on $PC4$ and $PC5$ are stable across the two samples using our data. This result is consistent with the stable loadings illustrated in Figures 5 and 6. However, with GSW data, the loading on $PC4$ ($PC5$) goes from -2.8 (-0.24) to 6.4 (14.7) from CP's original sample to the extended sample. Both the sign and the order of magnitude change, indicating the instability of the loadings.[20]

Overall, our data support CP's return-forecasting factor, and unspanned yield factors. By contrast, GSW data fail to provide coherent evidence to draw a conclusion in either direction.

5.2 Excess Volatility

GK document an excess volatility of long-term bond prices that cannot be explained by the discount-rate variation spanned by shorter-term bond prices.[21] Their analysis is based on the GSW data. We repeat their exercises with GSW data as well as our data.

In an affine term structure model, the short rate is affine in underlying latent factors x_t,

$$y_t(1) = \delta_0 + \delta_1' x_t, \tag{5.5}$$

---

[19]For Fama and Bliss (1987) data, the null hypothesis is rejected with CP's original sample, but we fail to reject the null with the extended sample using BH bootstrap p-values.

[20]Loadings associated with Fama and Bliss (1987) data also change size and sign, although the change is not as big as with the GSW data.

[21]Related work on excess volatility of long-run Treasury bond yields includes Gürkaynak et al. (2005) and Hanson and Stein (2015).

where δ_1 is a column vector.

The factor dynamics follow an AR(1) process under the risk-neutral measure $\mathbb{Q}$:

$$x_t = c^{\mathbb{Q}} + \rho^{\mathbb{Q}} x_{t-1} + \varepsilon_t. \tag{5.6}$$

As a result, log bond prices are affine in the latent factors,

$$\log P_t(n) = a_n + b_n' x_t, \tag{5.7}$$

where the loading b_n can be calculated recursively as

$$b_n' = b_{n-1}' \rho^{\mathbb{Q}} - \delta_1', \tag{5.8}$$

where $b_1 = -\delta_1$. For derivations, see Hamilton and Wu (2012, 2014). The identifying assumptions are $\rho^{\mathbb{Q}}$ is diagonal, $c^{\mathbb{Q}} = 0$, and $\delta_1 = [1, 1, 1]'$.

We follow GK's procedure to estimate $\rho^{\mathbb{Q}}$. First, we regress the log price of the seven-year zero-coupon bond $\log P_t(7)$ on the log prices of one-, three-, and five-year bonds: $\mathcal{P}_t = [\log P_t(1), \log P_t(3), \log P_t(5)]'$, and label the 3×1 slope $\hat{\beta}_7$. Then, we solve the three unknowns in $\rho^{\mathbb{Q}}$ from the three equations for $\hat{\beta}_7$:

$$\hat{\beta}_7 = [b_1, b_3, b_5]^{-1} b_7, \tag{5.9}$$

where the loadings b_1, b_3, b_5, b_7 are functions of $\rho^{\mathbb{Q}}$ through (5.8). This step of backing out the structural parameters from the reduced-form parameters follows Hamilton and Wu (2012). Let the estimated $\rho^{\mathbb{Q}}$ be $\hat{\rho}^{\mathbb{Q}}$.

For a long-term bond (GK use maturities of 20, 25, and 30 years; we also include 10 and 15 years), we can calculate the amount of price variation explained by $\mathcal{P}_t$ by imposing $\hat{\rho}^{\mathbb{Q}}$:

$$V^r(n) \equiv \mathbb{V}[\log P_t^r(n)] = \beta_n(\hat{\rho}^{\mathbb{Q}})' \mathbb{COV}[\mathcal{P}_t] \beta_n(\hat{\rho}^{\mathbb{Q}}), \tag{5.10}$$

where $\beta_n(\hat{\rho}^{\mathbb{Q}}) = [b_1(\hat{\rho}^{\mathbb{Q}}), b_3(\hat{\rho}^{\mathbb{Q}}), b_5(\hat{\rho}^{\mathbb{Q}})]^{-1} b_n(\hat{\rho}^{\mathbb{Q}})$. We refer to $V^r(n)$ as the restricted price variation.

Alternatively, we can run an unconstrained OLS regression of the long-term bond price on $\mathcal{P}_t$, and obtain the unrestricted regression coefficients $\hat{\beta}_n$ and hence the unrestricted price variation $V^u(n) \equiv \mathbb{V}[\log P_t^u(n)] = \hat{\beta}_n' \mathbb{COV}[\mathcal{P}_t] \hat{\beta}_n$. The ratio between the unrestricted and the restricted price variation, which is usually larger than 1, measures the degree of excess volatility:

$$\frac{V^u(n)}{V^r(n)} = \frac{\hat{\beta}_n' \mathbb{COV}[\mathcal{P}_t] \hat{\beta}_n}{\beta_n(\hat{\rho}^{\mathbb{Q}})' \mathbb{COV}[\mathcal{P}_t] \beta_n(\hat{\rho}^{\mathbb{Q}})}. \tag{5.11}$$

We carry out GK's analysis over both their original sample (i.e., 1985–2014) and our extended sample (1985–2019) at the daily frequency.[22] We use GK's bootstrap procedure to perform statistical inference, which is constructed under the null hypothesis of no excess volatility; that is, $\frac{V^u(n)}{V^r(n)} = 1$.

Figure 7 summarizes our findings. We plot the unrestricted price variations $V^u(n)$ in blue solid lines. Red dashed lines plot restricted price variations $V^r(n)$ with a 95% bootstrapped confidence band in the pink shaded area. The circles mark the maturities of interest, and the numbers above them are variance ratios $\frac{V^u(n)}{V^r(n)}$. Table 2 reports detailed testing results.

The top-right panel of Figure 7 uses GSW data to replicate GK's results for bonds with maturities of 20, 25, and 30 years. Our estimated variance ratios are almost identical to their reported estimates (see their Table II). Long-term bonds display excess volatilities as quantified by a variance ratio of 1.19, 1.38, and 1.62, respectively. Using our data, we find substantially larger estimates than using GSW data, as shown in the top-left panel. In particular, the three variance ratios for long-term bonds are 1.62, 2.02, and 2.37, respectively. Note GK show a variance ratio larger than 2 is routinely observed for other asset classes, but not for Treasuries. We show this result is driven by the GSW data they use. Using our data

---

[22]More specifically, our daily data go from November 29, 1985, to June 30, 2014, for GK's original sample, and from November 29, 1985, to December 31, 2019, for our extended sample.

Figure 7: **Excess Volatility**
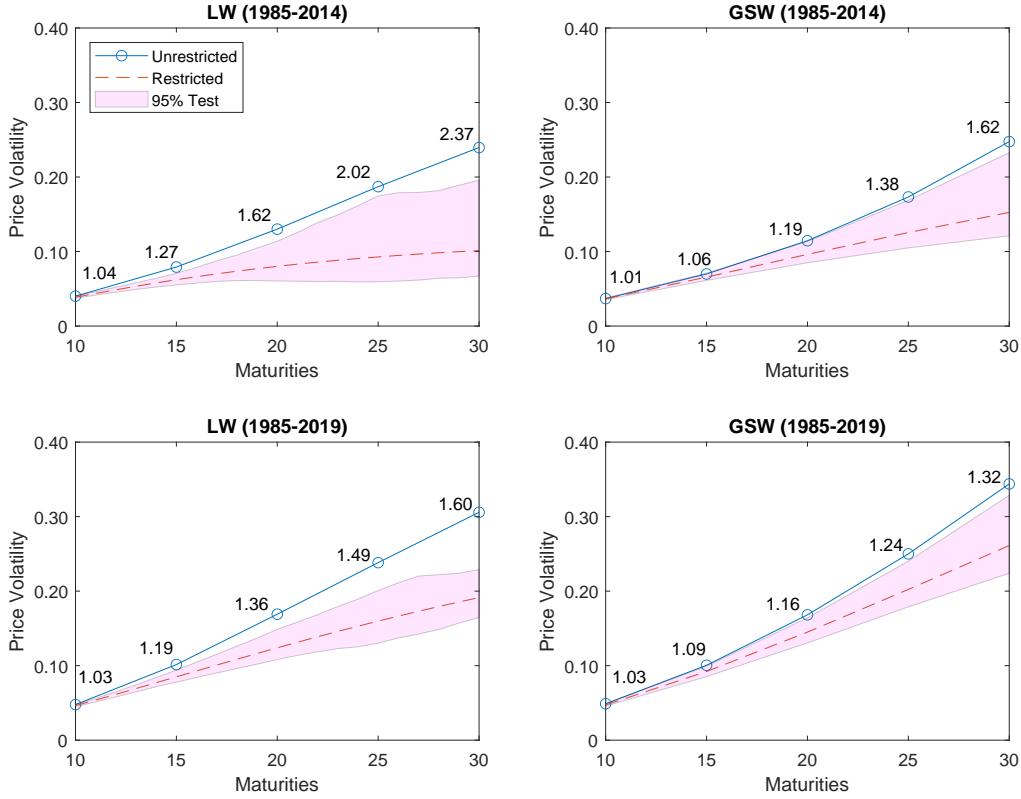
Notes: We plot the unrestricted variance $V^u(n)$ (solid line) and the restricted variance $V^r(n)$ (dashed line) for the log price of long-term bonds. The shaded area marks the 95% confidence bands. The circles highlight the variance ratios $\frac{V^u(n)}{V^r(n)}$ for bonds with selected maturities.

therefore helps GK reconcile the difference between Treasuries and other assets in terms of excess price volatility. Moreover, the gap between the blue line and the pink shaded area is also wider in the top-left panel. Overall, using our data strengthens GK's Treasury results and confirms their main conclusion.

Turning to the extended sample (bottom panels in Figure 7), variance ratios decline compared to the two panels at the top. This decline can be explained by low and less volatile interest rates caused by the zero lower bound starting from 2009.[23] Regardless, the

---

[23]During the 2009–2015 zero lower bound period, the short end of the yield curve is flat around zero, and does not display much variation. We find a reduction in both the restricted and the unrestricted price variation. However, the unrestricted variation drops more, resulting in a variance ratio of around 0.8 (in particular, 0.83 for 10-year, 0.78 for 15-year, 0.80 for 20-year, 0.77 for 25-year, and 0.87 for 30-year). Post 2015, the market continues to have small price variations under both the restricted and unrestricted model,

Table 2: **Testing Excess Volatility**

Original Sample (1985-2014)

	LW					GSW				
	10yr	*15yr*	*20yr*	*25yr*	*30yr*	*10yr*	*15yr*	*20yr*	*25yr*	*30yr*
Restricted	0.039	0.062	0.080	0.093	0.101	0.037	0.066	0.096	0.126	0.153
2.5% c.v.	0.037	0.057	0.064	0.064	0.072	0.036	0.061	0.085	0.105	0.121
97.5% c.v.	0.040	0.071	0.113	0.170	0.166	0.038	0.071	0.114	0.169	0.233
Unrestricted	0.040	0.079	0.130	0.187	0.240	0.037	0.070	0.115	0.173	0.248
Variance ratio	1.04	1.27	1.62	2.02	2.37	1.01	1.06	1.19	1.38	1.62
[*p*-value]	[0.02]	[0.00]	[0.00]	[0.01]	[0.00]	[0.37]	[0.08]	[0.01]	[0.01]	[0.01]

Extended Sample (1985-2019)

	LW					GSW				
Restricted	0.046	0.085	0.124	0.160	0.191	0.047	0.092	0.145	0.202	0.261
2.5% c.v.	0.045	0.078	0.108	0.133	0.163	0.046	0.085	0.131	0.179	0.224
97.5% c.v.	0.048	0.096	0.151	0.208	0.235	0.049	0.099	0.164	0.240	0.329
Unrestricted	0.048	0.102	0.169	0.238	0.306	0.049	0.101	0.168	0.250	0.344
Variance ratio	1.03	1.19	1.36	1.49	1.60	1.03	1.09	1.16	1.24	1.32
[*p*-value]	[0.05]	[0.00]	[0.00]	[0.00]	[0.00]	[0.01]	[0.01]	[0.00]	[0.00]	[0.00]

Notes: We compute the unrestricted variance $V^u(n)$ and the restricted variance $V^r(n)$ for the log price of long-term bonds. The variance ratios is $\frac{V^u(n)}{V^r(n)}$. *P*-values and 2.5% and 97.5% critical values are obtained through the bootstrap procedure of Giglio and Kelly (2018).

variance ratios estimated using our data remain larger than the ones implied by the GSW data.

Table 2 provides test results for the variance ratios. Besides the differences for maturities between 20 and 30 years that we highlight with Figure 7, we also find that with GK's original sample, a variance ratio of 1 is not rejected (at 5% level) for the 10-year and 15-year bonds using the GSW data, whereas it is rejected with our data. This observation further corroborates the ubiquity of excess volatility along the maturity spectrum, and demonstrates the difference between our data and the GSW data for bonds with intermediate maturities.

Overall, our data provide stronger support for GK's finding of excess volatility for long-

---

but the variance ratio is around 1 (in particular, 1.08 for 10-year, 1.04 for 15-year, 0.98 for 20-year, 0.88 for 25-year, and 0.94 for 30-year). Overall, the inclusion of the post-2015 sample for the extended sample generates a smaller variance ratio than the 1985–2014 sample. For further details on the zero lower bound, see Wu and Xia (2016).

term bond prices compared to the GSW data. The difference stems from the non-parametric method we use as opposed to the parametric approach adopted by GSW to construct the zero-coupon yield curve. In fact, the affine term structure model GK use implies a parametric yield curve with a few parameters. Suppose we use the GK model to construct the zero-coupon yield curve; then, by construction, the variance ratio for all long-term bonds is 1. By contrast, our nonparametric approach allows us to capture unique information that drives the movement of long-term bond prices, leading to a larger estimate of excess volatility.

6 Statistical Performance of the New Yield Curve

Section 5 discussed economic implications of our new yield curve, and this section turns to its statistical performance. Subsection 6.1 focuses on several selected dates to provide some intuition. Subsection 6.2 and Subsection 6.3 evaluate the goodness of fit more systematically, with the former examining summary statistics and the latter assessing the time series of pricing errors. Subsection 6.4 presents the out-of-sample results. We use monthly frequency for Subsection 6.2 and Subsection 6.3 and quarterly frequency for Subsection 6.4.

6.1 Yield Curves on Selected Dates

To gain some insights into the performance of our method, we use the yield to maturity (YTM) computed with the average price to compare our newly constructed yield curve with the raw data as well as the yield curve implied by GSW. For the raw data, the YTM is computed by (2.6). The model-implied YTM is the solution to (2.6), except the left-hand side is replaced with the model-implied price $\widehat{p}$, which is defined in (2.9) for our model.

Figure 8 illustrates the comparison for four dates: February 1968 (first column), July 2014 (second column), January 1990 (third column), and January 2010 (last column). The top row shows the zero-coupon yield curve; the next two rows are the YTM. Red indicates

observations, blue uses our method, and green is GSW.[24]

For February 1968, the main difference between our curve and GSW's is the short end. Whereas our zero-coupon yield approaches around 5% at a maturity of zero, it reaches a level of 15% for GSW's estimate. Importantly, as shown in panel (2,1) and more clearly in panel (3,1), the data do not support GSW's large estimate of the yield at the short end, leading to pricing errors that are in the magnitude of 20%.

The main difference between our model and GSW's in July 2014 is again the short end, which can be better seen in the (3,2) panel. This date lies inside the zero-lower-bound period (from 2009 to 2015). Our curve captures the pattern in the raw data and is consistent with the zero lower bound: the short end converges to zero when maturity approaches zero. By contrast, GSW has a U shape at the short end, and the difference in YTM between GSW and the raw data is about 0.3%.

Two explanations drive the above results on the short end. First, GSW drop raw data in the short end, including all observations with less than three months to maturity and all Treasury bills. Second, they use a parametric model. Consequently, fitting their parametric model mainly to securities with longer maturities may generate unstable and poorly identified estimates on the short end that are inconsistent with the data.[25] By contrast, our non-parametric method allows us to keep raw observations in the short end without sacrificing the fit for longer maturities.

For January 1990, the main difference is for longer maturities; see the (3,3) panel. The raw data display a humped shape, whereas GSW's estimate is monotonically increasing in maturity. Therefore, GSW generate pricing errors that are systematically positive between 300 and 350 months, and negative between 120 and 300 months. Note the 0.1% difference in YTM translates into a 0.5% difference in the zero-coupon yield. By contrast, our estimate fits the raw data well across all maturities.

---

[24]We reestimate GSW parameters based on our filtered raw data; see details in Appendix A.3. We also use GSW's published parameters (https://www.federalreserve.gov/data/nominal-yield-curve.htm) as a robustness check, and find the same results.

[25]See 5 of GSW for a related discussion on the instability of their estimates.

Figure 8: **Yield Curves on Selected Dates**
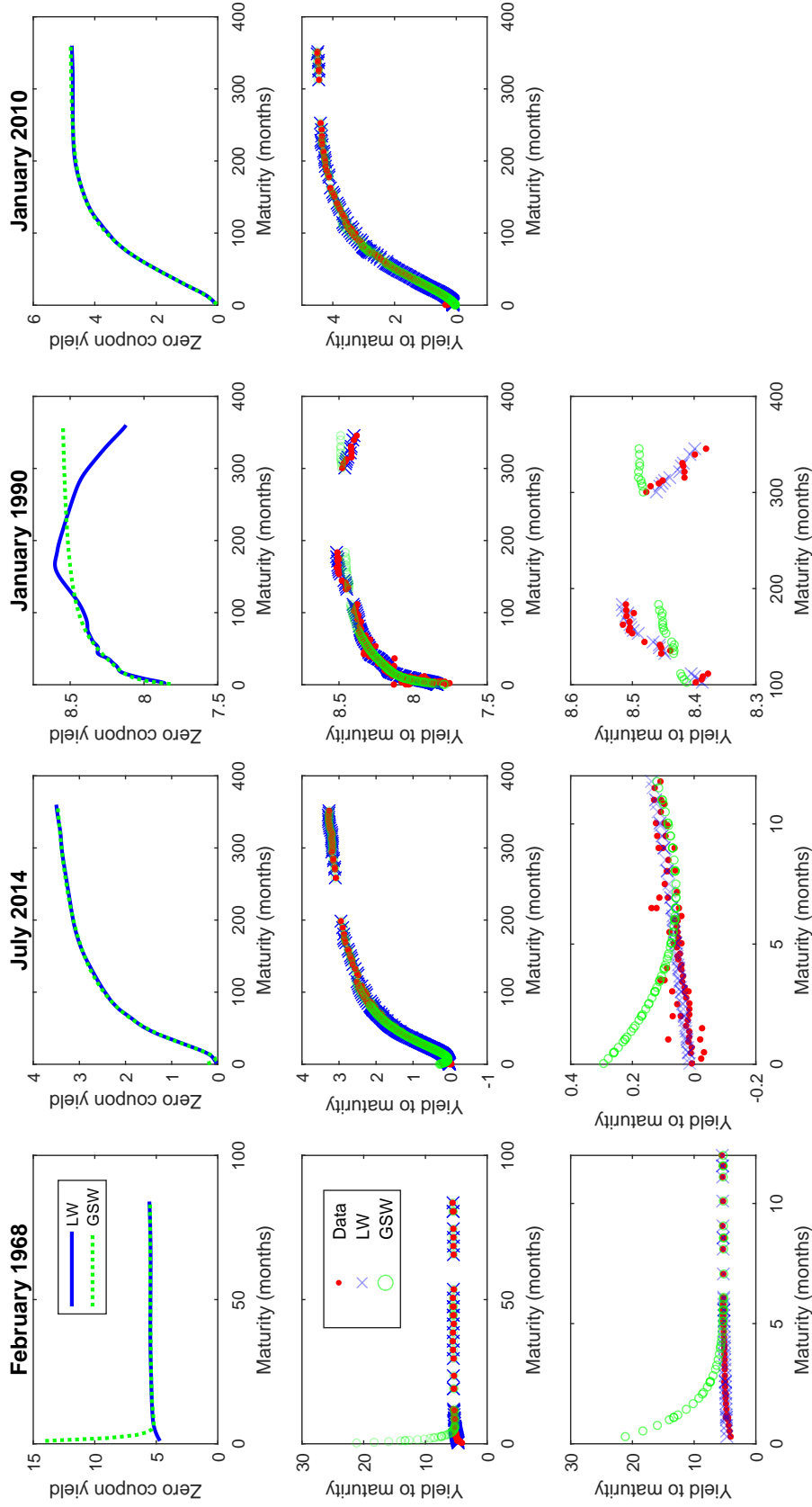
Notes: We plot the yield-curve estimates, as well as the implied yield to maturities (YTM) for four particular dates: February 1968, July 2014, January 1990, and January 2010. For each date, the top panels plot the two zero-coupon yield-curve estimates, one for our method ('LW') and one for GSW ('GSW'). The middle panels plot the YTM of the data (Data) as well as the implied YTM for our method (LW) and GSW (GSW) across all maturities. The bottom panels zoom into a certain maturity range to highlight the difference in YTM.

34

What drives the performance of GSW is the large gap in the maturity distribution, together with limited observations in the long end, which accounts for a large fraction of our data; see Figure 1. This feature, combined with parametric methods with a limited degree of freedom, leads to systematic pricing errors for bonds on both sides of the gap. By contrast, our framework allows us to flexibly capture the local variation of the yield curve before and after the gap, resulting in a substantial reduction in pricing errors.

Finally, the last date (January 2010) presents a time when our yield-curve estimate agrees with GSW's. Moreover, the implied YTMs from both methods also closely match the data. This example illustrates that our non-parametric method can produce a smooth yield curve and does not overfit.

6.2 Summary Statistics

This section systematically evaluates the performance of our dataset using the following metrics: root-mean-squared pricing error (RMSPE), duration-weighted root-mean-squared pricing error (WRMSPE), mean absolute pricing error (MAPE), duration-weighted mean absolute pricing error (WMAPE), and mean absolute yield error (MAYE). We also take bid-ask spread into account per Bliss (1996) and compile the corresponding MAPE (Bliss), WMAPE (Bliss), and the hit rate (HR (Bliss)). See their definitions in A.4. For the first seven, a smaller error indicates a better model, whereas a larger hit rate is associated with better performance.

Table 3 reports the performance comparison between our method and GSW for nine maturity buckets together with an overall comparison. Bold highlights the better performer. The top panel evaluates our method. In the bottom panel, we estimate GSW's curve with our filtered raw data.[26] As a robustness check, we also report results in Subsection B.3 using GSW's published parameters. Results remain the same.

---

[26]We follow GSW and add the following filter: drop all securities with maturities less than three months as well as Treasury bills.

Table 3: **In-Sample Performance Summary**

|				Maturity Bucket						All
	[0,3mth)	[3mth, 1yr)	[1yr, 2yr)	[2yr,5r)	[5yr, 7yr)	[7yr, 10yr)	[10yr, 15yr)	[15yr, 20yr)	[20yr, 30yr]	
LW										
RMSPE	0.016	0.043	0.079	0.148	0.242	0.399	0.406	0.189	0.117	0.167
WRMSPE	0.013	0.038	0.077	0.137	0.240	0.394	0.404	0.190	0.118	0.055
MAPE	0.013	0.033	0.062	0.108	0.199	0.341	0.358	0.157	0.092	0.088
WMAPE	0.010	0.028	0.061	0.100	0.197	0.336	0.356	0.158	0.092	0.023
MAPE (Bliss)	0.006	0.016	0.032	0.063	0.139	0.261	0.260	0.111	0.059	0.055
WMAPE (Bliss)	0.005	0.014	0.030	0.057	0.138	0.256	0.258	0.112	0.059	0.012
MAYE	0.108	0.063	0.045	0.035	0.041	0.053	0.045	0.013	0.006	0.054
HR (Bliss)	0.405	0.407	0.520	0.398	0.297	0.208	0.273	0.311	0.353	0.407
GSW										
RMSPE	0.042	0.058	0.093	0.188	0.325	0.542	0.635	0.453	0.455	0.257
WRMSPE	0.037	0.053	0.091	0.176	0.323	0.534	0.629	0.455	0.453	0.088
MAPE	0.038	0.046	0.075	0.140	0.276	0.473	0.559	0.411	0.398	0.139
WMAPE	0.031	0.042	0.073	0.130	0.274	0.466	0.553	0.413	0.396	0.044
MAPE (Bliss)	0.029	0.029	0.041	0.092	0.214	0.387	0.455	0.357	0.359	0.104
WMAPE (Bliss)	0.025	0.027	0.040	0.084	0.212	0.379	0.448	0.359	0.357	0.032
MAYE	0.336	0.095	0.054	0.046	0.056	0.073	0.069	0.032	0.027	0.116
HR (Bliss)	0.243	0.340	0.402	0.296	0.184	0.112	0.149	0.110	0.125	0.282

Notes: We present results for two models: LW (our model) and GSW. For each maturity bucket (or across all bonds) and for each date, we calculate eight measures of pricing error: root-mean-squared pricing error (RMSPE), duration-weighted root-mean-squared pricing error (WRMSPE), mean absolute pricing error (MAPE), duration-weighted absolute pricing error (WMAPE), mean absolute pricing error adjusted for bid-ask spread (MAPE (Bliss)), duration-weighted absolute pricing error adjusted for bid-ask spread (WMAPE (Bliss)), mean absolute yield error (MAYE), and the hit rate (HR (Bliss)). RMSPE, WRMSPE, MAPE, WMAPE, MAPE (Bliss), and WMAPE (Bliss) are based on a face value of $100. MAYE is based on annualized percentage yield. We report the average pricing errors from June 1961 to December 2019.

Our method performs better than GSW across all metrics and maturity buckets. The improvement is substantial, and the reduction in pricing errors across all bonds (last column) ranges between 35% and 62%, with the largest reduction occurring in WMAPE (Bliss).

Across maturity buckets, our model performs significantly better at the short end and the longer end. For maturities less than three months, the percentage reduction in the pricing error of our model relative to GSW ranges from 62% to 80%, with WMAPE (Bliss) implying the largest reduction.

For maturities above five years, our model again presents a substantial improvement over GSW. The percentage reduction in pricing error ranges from 26% to 33% over the maturity

Figure 9: **Time Series of Mean Absolute Error in YTM: The Short End**
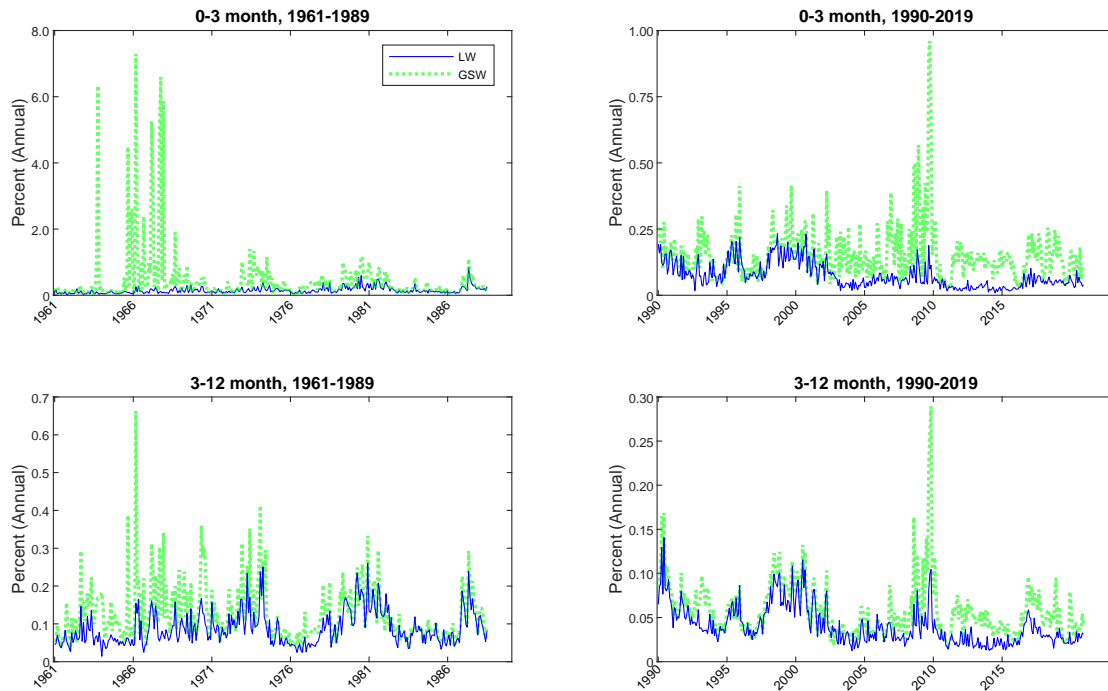
Notes: We plot the mean absolute pricing errors in YTM (i.e., MAYE) for our method and GSW over the entire sample period (i.e., 1961–2019). The top panel examines bonds with maturities less than three months; the bottom panel examines bonds with maturities between three months and one year.

range between 5 years and 10 years, from 45% to 54% between 10 years and 20 years, and 74% to 84% between 20 years and 30 years.

6.3 Time-Series Evidence

This section examines the time series of pricing errors to provide more insights into the performance of our method.

The short term Figure 9 shows our model performs consistently better than GSW across different time periods for maturities less than one year. The top panel plots maturities less than three months, and the bottom panel plots maturities between three months and one year. We split the full sample into the 1961–1989 (left panels) and the 1990–2019 (right

panels) sub-samples given the general decline in pricing error over time.[27]

For maturities less than three months (top panels), we observe that GSW occasionally generate large pricing errors at around 7 annualized percentage points. The left column of Figure 8 illustrates one such example in February 1968. We see a general decline in pricing error over the post-1990 period. However, GSW's pricing error can still reach 1%. Our method is able to reduce these pricing errors significantly.

For maturities between three months and one year (bottom panels), our model continues to outperform GSW. In particular, our model does better than GSW for the 1961-1975 period and the more recent post-2009 period. The post-2009 period is associated with the zero lower bound and subsequent low-interest-rate environment. As in the second column of Figure 8, we have illustrated that our method fits the short end of the yield curve better for this special period in history.[28]

The large pricing errors of GSW at the short end come from the fact that they exclude all securities with less than three months to maturity as well as all Treasury bills. Consequently, GSW extrapolate the short end of the yield curve from securities with longer maturities, which leads to imprecise and sometimes extreme estimates of the short end of the yield curve.

Moreover, the issue of the short end of the yield curve of GSW is unlikely to be solved by simply including securities with short maturities in their estimation. The challenge is that the parametric model used in GSW has a limited degree of freedom and cannot simultaneously capture short-term, medium-term, and long-term yields.

By contrast, our non-parametric framework with adaptive bandwidth presents a natural solution to this challenge, because it adjusts the amount of local information used to construct the yield curve.

---

[27]To ensure that reestimating GSW's parameters based on our data does not cause the large pricing errors for their model, we plot the minimum pricing error between their original and our re-estimated versions in Figure 9.

[28]The superior performance of the short end of our yield curve data makes it particularly useful for studies that try to disentangle short-rate expectations and risk premiums in driving bond returns (see Cieslak (2018) for a recent application).

The Medium and Long Term For maturities between one and five years, our model performs similarly to GSW, with the exception of the post-2009 sample; see Figure B.3 for illustration. During the low-interest-rate period after 2009, our model significantly outperforms GSW's. The similarity in performance before that period is consistent with the observation that abundant data are available over this maturity range, causing parametric models such as GSW's to use most of its degree of freedom to fit this part of the data.

For maturities above five years, we again see substantial improvement of our model over GSW; see Figure B.4 for more details. Between 5 years and 10 years, we start to see the improvement of our method. For example, between 2000 and 2006, we are able to reduce the MAYE from 0.08% in GSW to around 0.02%.

The pricing errors of GSW for maturities longer than 10 years contain large spikes. For example, between 1986 and 1990, GSW's pricing error for maturities between 20 years and 30 years reaches 0.3%. By contrast, the pricing error from our method always stays under 0.05%. Moreover, our improvement applies not only to the pre-1990 sample for which a limited number of long-term securities are outstanding, but also to the post-1990 sample, including the most recent sample when abundant data on the long end are available.

6.4   Out-of-Sample Results

We have shown the superior in-sample performance of our non-parametric method. We next examine its out-of-sample performance to address the overfitting concern for non-parametric methods. We construct our out-of-sample prediction exercise as follows. On each date, we estimate the yield curve I_t times, where I_t is the number of Treasury securities we observe at t. Each time, we leave out a bond i and use the remaining bonds to compute the model-implied price for bond i and hence its out-of-sample pricing error using the same eight metrics as in Subsection 6.2. We repeat this exercise over t to calculate the average pricing error. Given the computational burden of the out-of-sample exercise, we use quarterly sample from

Table 4: **Out-of-Sample Performance Comparison**

	Maturity Bucket									All
	[0,3mth)	[3mth, 1yr)	[1yr, 2yr)	[2yr,5r)	[5yr, 7yr)	[7yr, 10yr)	[10yr, 15yr)	[15yr, 20yr)	[20yr, 30yr]	
LW										
RMSPE	0.016	0.045	0.090	0.175	0.299	0.478	0.578	0.246	0.162	0.208
WRMSPE	0.013	0.039	0.088	0.162	0.297	0.472	0.576	0.247	0.162	0.064
MAPE	0.013	0.034	0.071	0.126	0.247	0.404	0.517	0.203	0.126	0.103
WMAPE	0.010	0.029	0.069	0.116	0.245	0.399	0.514	0.204	0.126	0.024
MAPE (Bliss)	0.006	0.017	0.039	0.079	0.185	0.324	0.411	0.156	0.091	0.070
WMAPE (Bliss)	0.005	0.014	0.037	0.071	0.183	0.319	0.409	0.157	0.091	0.013
MAYE	0.110	0.065	0.052	0.041	0.051	0.063	0.065	0.016	0.009	0.057
HR (Bliss)	0.409	0.398	0.490	0.361	0.229	0.175	0.210	0.252	0.274	0.384
GSW										
RMSPE	0.038	0.050	0.094	0.198	0.344	0.564	0.628	0.476	0.468	0.293
WRMSPE	0.032	0.047	0.092	0.185	0.342	0.555	0.624	0.478	0.465	0.095
MAPE	0.035	0.040	0.076	0.147	0.294	0.491	0.541	0.429	0.403	0.165
WMAPE	0.027	0.037	0.074	0.137	0.292	0.483	0.538	0.432	0.401	0.044
MAPE (Bliss)	0.030	0.015	0.041	0.099	0.231	0.404	0.436	0.375	0.365	0.124
WMAPE (Bliss)	0.024	0.013	0.040	0.090	0.229	0.395	0.433	0.377	0.362	0.032
MAYE	0.324	0.070	0.054	0.048	0.059	0.076	0.067	0.032	0.027	0.113
HR (Bliss)	0.109	0.541	0.386	0.282	0.168	0.102	0.147	0.093	0.119	0.286

Notes: We present results for two models: LW (our model) and GSW. For each maturity bucket (or across all bonds) and for each date, we calculate eight measures of pricing error: root-mean-squared pricing error (RMSPE), duration-weighted root-mean-squared pricing error (WRMSPE), mean absolute pricing error (MAPE), duration-weighted absolute pricing error (WMAPE), mean absolute pricing error adjusted for bid-ask spread (MAPE (Bliss)), duration-weighted absolute pricing error adjusted for bid-ask spread (WMAPE (Bliss)), mean absolute yield error (MAYE), and the hit rate (HR (Bliss)). RMSPE, WRMSPE, MAPE, WMAPE, MAPE (Bliss), and WMAPE (Bliss) are based on a face value of $100. MAYE is based on annualized percentage yield. We report the averaged pricing errors over the full sample from June 1961 to December 2019 at the quarterly frequency.

June 1961 to December 2019.[29]

We report in Table 4 the out-of-sample comparison between our approach at the optimal $N_0 = 8$ and GSW's. The out-of-sample result is similar to the in-sample comparison in Table 3: our method produces uniformly smaller pricing errors and a higher hit rate across maturity buckets. For example, the average reduction in MAYE is 49%.

We also compare alternative values for N_0 to search for the optimal bandwidth; see details in Subsection B.5. Different N_0 does not significantly change the relative performance

---

[29]For each of the four model specifications, the out-of-sample exercise takes about a week for a computer with dual Intel Xeon Gold 6136 CPU and 208 GB memory using 24 workers in MATLAB parallel computing.

between our approach and GSW's. Across different values, $N_0 = 8$ generates the smallest pricing error in terms of RMSPE, and leads to a smoother yield curve than smaller N_0 values. We therefore consider $N_0 = 8$ the optimal bandwidth parameter.

7   Conclusion

The zero-coupon yield curve provides important information about financial markets and the macroeconomy, and is widely used by researchers and practitioners. Our paper develops a new dataset using a non-parametric kernel-smoothing method with a novel adaptive bandwidth specifically designed to fit the Treasury yield curve. Our method allows us to generate a smoothed yield curve while preserving the information in the raw data. We show our yield-curve estimate provides a more accurate description of the raw data than the leading alternative GSW. Economically, we show that applying our data draws different conclusions from GSW when we repeat two popular studies by CP and GK.

References

Ang, Andrew and Monika Piazzesi, "A no-arbitrage vector autoregression of term structure dynamics with macroeconomic and latent variables," *Journal of Monetary Economics*, 2003, *50*, 745–787.

Bauer, Michael D and James D Hamilton, "Robust bond risk premia," *The Review of Financial Studies*, 2018, *31* (2), 399–448.

Bauer, Michael D., Glenn D. Rudebusch, and Jing Cynthia Wu, "Correcting Estimation Bias in Dynamic Term Structure Models," *Journal of Business & Economic Statistics*, 2012, *30* (3), 454–467.

_ , _ , **and** _ , "Term premia and inflation uncertainty: empirical evidence from an international panel dataset: comment," *American Economic Review*, 2014, *1* (104), 323–337.

Bernanke, Ben S and Vincent R Reinhart, "Conducting monetary policy at very low short-term interest rates," *American Economic Review*, 2004, *94* (2), 85–90.

Bliss, Robert R, "Testing term structure estimation methods," Technical Report, Working Paper, Federal Reserve Bank of Atlanta 1996.

Cieslak, Anna, "Short-rate expectations and unexpected returns in treasury bonds," *The Review of Financial Studies*, 2018, *31* (9), 3265–3306.

_ **and Hao Pang**, "Common shocks in stocks and bonds," 2020.

_ **and Pavol Povala**, "Expected returns in Treasury bonds," *The Review of Financial Studies*, 2015, *28* (10), 2859–2901.

Cochrane, John H, "Comments on "Robust Bond Risk Premia" by Michael Bauer and Jim Hamilton," *Unpublished working paper. University of Chicago*, 2015.

___ **and Monika Piazzesi**, "Bond risk premia," *American Economic Review*, 2005, *95* (1), 138–160.

Cooper, Ilan and Richard Priestley, "Time-varying risk premiums and the output gap," *The Review of Financial Studies*, 2009, *22* (7), 2801–2833.

Diebold, Francis X. and Glenn D. Rudebusch, *Yield Curve Modeling and Forecasting.*, Princeton, NJ: Princeton University Press, 2013.

Duffee, Gregory R., "Term premia and interest rate forecasts in affine models," *The Journal of Finance*, 2002, *57* (1), 405–443.

___ , "Information in (and not in) the term structure," *The Review of Financial Studies*, 2011, *24* (9), 2895–2934.

Fama, Eugene and Robert R Bliss, "The Information in Long-Maturity Forward Rates," *American Economic Review*, 1987, *77* (4), 680–92.

Fama, Eugene F, "Term premiums in bond returns," *Journal of Financial economics*, 1984, *13* (4), 529–546.

Fan, Jianqing and Irene Gijbels, "Data-driven bandwidth selection in local polynomial fitting: variable bandwidth and spatial adaptation," *Journal of the Royal Statistical Society. Series B (Methodological)*, 1995, pp. 371–394.

Giglio, Stefano and Bryan Kelly, "Excess volatility: Beyond discount rates," *The Quarterly Journal of Economics*, 2018, *133* (1), 71–127.

Greenwood, Robin and Dimitri Vayanos, "Bond supply and excess bond returns," *The Review of Financial Studies*, 2014, *27* (3), 663–713.

Gürkaynak, Refet S, Brian Sack, and Eric Swanson, "The sensitivity of long-term interest rates to economic news: Evidence and implications for macroeconomic models," *American economic review*, 2005, *95* (1), 425–436.

Gürkaynak, Refet S., Brian Sack, and Jonathan H. Wright, "The U.S. Treasury Yield Curve: 1961 to the Present," *Journal of Monetary Economics*, November 2007, *54* (8), 2291–2304.

Hamilton, James D. and Jing Cynthia Wu, "Identification and estimation of Gaussian affine term structure models," *Journal of Econometrics*, 2012, *168* (2), 315–331.

_ **and** _ , "Testable implications of affine term structure models," *Journal of Econometrics*, 2014, *178*, 231–242.

Hanson, Samuel G and Jeremy C Stein, "Monetary policy and long-term real rates," *Journal of Financial Economics*, 2015, *115* (3), 429–448.

Hodrick, Robert J and Tuomas Tomunen, "Taking the Cochrane-Piazzesi Term Structure Model Out of Sample: More Data, Additional Currencies, and FX Implications," Working Paper 25092, National Bureau of Economic Research September 2018.

Hull, John and Alan White, "Pricing interest-rate-derivative securities," *The Review of Financial Studies*, 1990, *3* (4), 573–592.

Jarrow, Robert and Yildiray Yildirim, "Pricing treasury inflation protected securities and related derivatives using an HJM model," *Journal of Financial and Quantitative Analysis*, 2003, *38* (2), 337–358.

Jeffrey, Andrew, Oliver Linton, and Thong Nguyen, "Flexible Term Structure Estimation: Which Method is Preferred?," *Metrika*, Feb 2006, *63* (1), 99–122.

Joslin, Scott, Marcel Priebsch, and Kenneth J Singleton, "Risk premiums in dynamic term structure models with unspanned macro risks," *The Journal of Finance*, 2014, *69* (3), 1197–1233.

Koijen, Ralph SJ, Hanno Lustig, and Stijn Van Nieuwerburgh, "The cross-section and time series of stock and bond returns," *Journal of Monetary Economics*, 2017, *88*, 50–69.

Linton, Oliver, Enno Mammen, Jans Perch Nielsen, and Carsten Tanggaard, "Yield curve estimation by kernel smoothing methods," *Journal of Econometrics*, 2001, *105* (1), 185–223.

Ludvigson, Sydney C and Serena Ng, "Macro factors in bond risk premia," *The Review of Financial Studies*, 2009, *22* (12), 5027–5067.

Nelson, Charles R. and Andrew Siegel, "Parsimonious modelling of yield curves," *Journal of Business*, 1987, *60* (4), 473–489.

Park, Byeong U and James S Marron, "Comparison of data-driven bandwidth selectors," *Journal of the American Statistical Association*, 1990, *85* (409), 66–72.

Rudebusch, Glenn D, "Term structure evidence on interest rate smoothing and monetary policy inertia," *Journal of monetary economics*, 2002, *49* (6), 1161–1187.

Ruppert, David, Simon J Sheather, and Matthew P Wand, "An effective bandwidth selector for local least squares regression," *Journal of the American Statistical Association*, 1995, *90* (432), 1257–1270.

Svensson, Lars E.O., "Estimating and Interpreting Forward Interest Rates: Sweden 1992 - 1994," Working Paper 4871, National Bureau of Economic Research September 1994.

Tukey, John W, *Exploratory data analysis*, Vol. 2, Reading, Mass., 1977.

Wand, Matt P and M Chris Jones, *Kernel smoothing*, CRC press, 1994.

Wu, Jing Cynthia and Fan Dora Xia, "Measuring the Macroeconomic Impact of Monetary Policy at the Zero Lower Bound," *Journal of Money, Credit, and Banking*, 2016, *48* (2-3), 253–291.

A Details on Implementation

A.1 Derivation and Estimation

The first-order conditions for the minimization problem in (2.7) are

$$\sum_{i=1}^{I}\sum_{j=1}^{J_i}\Phi_j^i(n;y,y')\cdot 1/D_i^2 \;=\; 0, \tag{A.1}$$

$$\sum_{i=1}^{I}\sum_{j=1}^{J_i}\Phi_j^i(n;y,y')(n-\nu_j^i)\cdot 1/D_i^2 \;=\; 0, \tag{A.2}$$

where $\Phi_j^i(n;y,y')$ is given by

$$
\Phi_j^i(n;y,y') \;=\; \Big(K_{h(\nu_j^i)}(n-\nu_j^i)c_j^i\nu_j^i d_j^i(n)\Big)
$$
$$
\times\left(p^i - c_j^i d_j^i(n) - \sum_{\substack{k=1\\k\neq j}}^{J_i}\Big(\int K_{h(\nu_k^i)}(n-\nu_k^i)c_k^i d_k^i(n)dn\Big)\right), \tag{A.3}
$$
$$
d_k^i(n) \;=\; \exp\left[-\Big(y(n)+(\nu_k^i-n)y'(n)\Big)\nu_k^i\right]. \tag{A.4}
$$

Note equation (A.3) (and therefore equations (A.1) and (A.2)) contains integrals. Although, in principle, solving equations (A.1) and (A.2) numerically is possible,[30] we follow Jeffrey et al. (2006) and approximate the integrals with interpolations that are functions of $y(\cdot)$ and $y'(\cdot)$.[31]

In particular, suppose the support of $y(\cdot)$ and $y'(\cdot)$ is $\mathcal{N}=\{1,2,...,360\}$. We approximate

---

[30]See Linton et al. (2001) for the iterative algorithms they propose to solve a system of equations that are similar to equations (A.1) and (A.2).

[31]We implemented both Linton et al. (2001) (in particular, the log-linear specification) and Jeffrey et al. (2006) for our model. Our experience is that Jeffrey et al. (2006) indeed offer a more stable and computationally efficient solution than Linton et al. (2001).

the integrals in equation (A.3) as

$$\int K_{h(\nu_k^i)}(n - \nu_k^i) d_k^i(n) dn$$

$$\approx \frac{\sum_{n=1}^{360} K_{h(\nu_k^i)}(n - \nu_k^i) \exp\left[-\left(y(n) + (\nu_k^i - n)y'(n)\right)\nu_k^i\right]}{\sum_{n=1}^{360} K_{h(\nu_k^i)}(n - \nu_k^i)}. \tag{A.5}$$

On the other hand, viewing $d_k^i(n)$ as the discount rate at ν_k^i approximated by the yield curve at n, $\int K_{h(\nu_k^i)}(n - \nu_k^i) d_k^i(n) dn$ can be interpreted as the kernel-smoothed discount rate at ν_k^i. Letting the corresponding zero-coupon yield be $\widehat{y}(\nu_k^i)$, which is defined through $\int K_{h(\nu_k^i)}(n - \nu_k^i) d_k^i(n) dn = \exp[-\nu_k^i \times \widehat{y}(\nu_k^i)]$, we obtain $\widehat{y}(\nu_k^i)$ as[32]

$$\widehat{y}(\nu_k^i) = -\frac{1}{\nu_k^i} \log\left(\frac{\sum_{n=1}^{360} K_{h(\nu_k^i)}(n - \nu_k^i) \exp\left[-\left(y(n) + (\nu_k^i - n)y'(n)\right)\nu_k^i\right]}{\sum_{n=1}^{360} K_{h(\nu_k^i)}(n - \nu_k^i)}\right). \tag{A.6}$$

Replacing ν_k^i by an arbitrary maturity ν in (A.6), we arrive at the formula that we use to interpolate the yield curve at any maturity ν.

In sum, we seek to solve equations (A.1) and (A.2) with respect to $y(n)$ and $y'(n)$ for $n \in \mathcal{N} = \{1, 2, ..., 360\}$, where $\Phi_j^i(n; y, y')$ is given by equations (A.3) and (A.4), but with the integrals in equation (A.3) replaced by equations (A.5) and (A.6). In essence, we are solving a system of non-linear equations. By construction, all of these equations involve functions that are infinitely differentiable. We provide closed-form gradients for these equations,[33] which allows us to solve these non-linear equations efficiently.

---

[32] The above interpolation can be interpreted as the solution to an optimization problem that is similar to (2.7) for a pure discount bond with a maturity of ν_k^i. More specifically, for a given estimated $\widetilde{y}(\cdot)$ and $\widetilde{y}'(\cdot)$, the solution to the minimization problem $\min_{y(\nu_k^i)} \int \left(\exp\left[-y(\nu_k^i) \times \nu_k^i\right] - \exp\left[-\left(\widetilde{y}(n) + (\nu_k^i - n)\widetilde{y}'(n)\right)n\right]\right)^2 K_{h(\nu_k^i)}(n - \nu_k^i) dn$ is given by $y(\nu_k^i) = -\frac{1}{\nu_k^i} \log\left(\int \left(\exp\left[-\left(\widetilde{y}(n) + (\nu_k^i - n)\widetilde{y}'(n)\right)n\right]\right) K_{h(\nu_k^i)}(n - \nu_k^i) dn\right)$. Because we only have solutions for $\widetilde{y}(\cdot)$ and $\widetilde{y}'(\cdot)$ over $\mathcal{N} = \{1, 2, ..., 360\}$, the interpolated version of this solution is given by equation (A.6).

[33] This is another benefit of replacing the integrals in equation (A.3) with interpolated yields as in equation (A.6).

A.2 Outlier Detection

Our outlier-detection algorithm follows several steps.

First, we drop observations whose yield to maturity (YTM) is higher than 30% (annualized). In the data, sometimes bond price appears to be too low (equivalently, YTM appears to be too high). Across time, bond prices in general reach their lowest during the early 1980s recession, approaching a level of 20% in YTM. We therefore set $30\% = 1.5 \times 20\%$ as a lenient threshold in YTM to drop low-price observations. Note potential outliers that have a high YTM but still below 30%, which are not dropped after this step, are likely to be dropped after the following steps.

Next, suppose the current day is t. We obtain our nonparametric yield-curve estimate from day $t-1$. Based on this estimate, we calculate the implied YTM for all bond observations for day t (denoted as $\widehat{YTM}_{i,t-1}$ for bond i). Assuming yield curves are internally consistent across days and therefore display relatively small day-to-day variations, we take $\widehat{YTM}_{i,t-1}$ as the benchmark YTM and evaluate the distance between $YTM_{i,t}$ (i.e., current YTM for bond i) and $\widehat{YTM}_{i,t-1}$. A bond with a large distance is a suspect outlier.

To take into account the difference in data quality (i.e., noise level) in different maturity segments, we group bonds into several maturity ranges. For each maturity range and for each bond within, we calculate $Dist_{i,t} \equiv |YTM_{i,t} - \widehat{YTM}_{i,t-1}|$. We use $\pm Dist_{i,t}$ for all bonds within the maturity range, and calculate the interquartile range (IQR, i.e., the $75th$ percentile minus the $25th$ percentile). An outlier is detected if its current-day YTM (i.e., $YTM_{i,t}$) is either below $\widehat{YTM}_{i,t-1} - 3 \times IQR$ or above $\widehat{YTM}_{i,t-1} + 3 \times IQR$. We choose three (rather than 1.5 as usual for outlier detection; see, e.g., Tukey (1977)) to be conservative in excluding bond observations. We also choose three maturity segments: bonds with a maturity of less than one year, between one year and five years, and above five years. Our 3.0-IQR rule applied to segment-specific data allows us to keep as much data as possible. Bond observations that are identified as outliers often have large discrepancy (in terms of yield to maturity) from other observations that have similar maturities.

A.3 Our Implementation of GSW

We obtain GSW's parameters from the Federal Reserve Board's webpage, and use them as starting values and re-estimate their model based on our raw bond data. Besides applying our filters described in Subsection 4.1, we also drop securities with less than three months to maturity and all Treasury bills, following GSW. In addition, we follow GSW by using the Nelson-Siegel four-parameter specification for the period before 1980 and GSW's six-parameter specification for the post-1980 period.

For most months, the re-estimated GSW curve is very similar to their original curve computed using their published parameters. This finding confirms the similarity in the underlying raw data we use. For a few months, the two versions have a substantial difference in the short end, where observations are omitted in estimation following GSW. This instability is consistent with what GSW find; see Section 5 of their paper. Given the parameter instability of GSW, we compare our method with both the re-estimated GSW and their reported parameters.

A.4 Model-Comparison Metrics

Let the actual bond price and the model-implied bond price be p_i and $\widehat{p}_i$ for $i = 1, 2, ..., I$. We first define two measures of pricing error that are directly related to our objective function. The first is the root-mean-squared pricing error (RMSPE) that calculates the square root of the mean-squared distance between p_i and $\widehat{p}_i$, that is, $\sqrt{\frac{1}{I} \sum_{i=1}^{I} (p_i - \widehat{p}_i)^2}$. The second is the duration-weighted root-mean-squared pricing error (WRMSPE) defined as $\sqrt{\frac{1}{I} \sum_{i=1}^{I} w_i^2 (p_i - \widehat{p}_i)^2}$, where $w_i = \frac{D_i^{-1}}{\sum_{i=1}^{I} D_i^{-1}}$ is the weight for bond i. Note WRMSPE is equivalent to our objective function that also weights pricing errors by bond durations.

We next define two metrics related to absolute pricing errors. They are the mean absolute pricing error, $\text{MAPE} = \frac{1}{I} \sum_{i=1}^{I} |p_i - \widehat{p}_i|$, and the duration-weighted mean absolute pricing error, $\text{WMAPE} = \sum_{i=1}^{I} w_i |p_i - \widehat{p}_i|$.

Bliss (1996) argues the bid-ask spread needs to be taken into account when calculating the pricing error. We follow Bliss (1996) to define the bid-ask-spread-adjusted pricing error as

$$
\varepsilon_i = \begin{cases} \widehat{p}_i - p_i^a & \text{if } \widehat{p}_i > p_i^a, \\ p_i^b - \widehat{p}_i & \text{if } \widehat{p}_i < p_i^b, \\ 0 & \text{otherwise,} \end{cases}
$$

where p_i^a and p_i^b are the ask and bid quotes, respectively, for the bond. The corresponding mean absolute pricing error (denoted as MAPE (Bliss)) and duration-weighted absolute pricing error (denoted as WMAPE (Bliss)) are defined as $\frac{1}{I} \sum_{i=1}^{I} \varepsilon_i$ and $\sum_{i=1}^{I} w_i \varepsilon_i$.

Next, rather than calculating the error between the actual and the fitted price, we define the mean absolute yield error (MAYE) as the average absolute error between the observed and the fitted YTM.

Lastly, we follow Bliss (1996) to define the hit rate (HR (Bliss)) as $\frac{1}{I} \sum_{i=1}^{I} \mathbb{1}_{\{p_i^b \le \widehat{p}_i \le p_i^a\}}$, where $\mathbb{1}_{\{p_i^b \le \widehat{p}_i \le p_i^a\}}$ is the indicator function that equals 1 if $\widehat{p}_i$ falls within $[p_i^b, p_i^a]$. The hit rate calculates the number of times the fitted price falls within the bid-ask spread.

B   Additional Results

B.1   CP Regressions with Fama-Bliss Data

Figure B.1: **CP Loadings with Fama-Bliss Data**
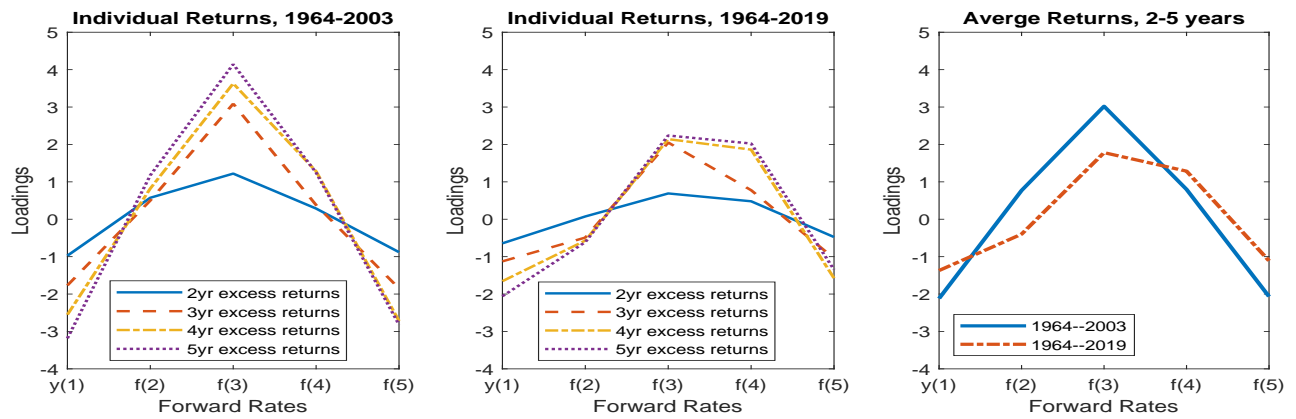
Notes: X-axis: independent variables $y_t(1), f_t(2), ..., f_t(5)$.

Table B.1: **CP Regression Results with Fama-Bliss Data (Predicting 2- to 5-Year Bond Returns)**

Fama-Bliss Data

|		Forward Rates					PCs					R-square
		$y(1)$	$f(2)$	$f(3)$	$f(4)$	$f(5)$	$PC1$	$PC2$	$PC3$	$PC4$	$PC5$	
(1964-2003)	Loadings	-2.119	0.769	3.021	0.798	-2.067	0.168	-1.459	-2.624	3.143	0.437	0.351
	NW t-stat	-6.193	1.112	5.460	1.750	-4.997	2.190	-4.373	-6.237	4.981	0.570	
	[NW p-value]	[0.00]	[0.27]	[0.00]	[0.08]	[0.00]	[0.03]	[0.00]	[0.00]	[0.00]	[0.57]	
	BH 5% c.v.	4.819	2.429	2.682	2.991	2.580	4.134	6.578	2.744	2.745	2.227	
	[BH p-value]	[0.01]	[0.37]	[0.00]	[0.28]	[0.00]	[0.38]	[0.27]	[0.00]	[0.00]	[0.61]	
	F-stat									21.099		
	[p-value]									[0.00]		
	BH 5% c.v.									8.061		
	[BH p-value]									[0.00]		
(1964-2019)	Loadings	-1.371	-0.399	1.781	1.286	-1.111	0.061	-1.254	-2.188	0.933	-0.928	0.228
	NW t-stat	-3.161	-0.603	2.561	3.026	-2.385	1.043	-4.038	-4.162	1.277	-1.202	
	[NW p-value]	[0.00]	[0.55]	[0.01]	[0.00]	[0.02]	[0.30]	[0.00]	[0.00]	[0.20]	[0.23]	
	BH 5% c.v.	4.597	2.178	2.489	3.150	2.863	3.806	6.705	2.755	2.253	2.097	
	[BH p-value]	[0.25]	[0.59]	[0.04]	[0.06]	[0.10]	[0.67]	[0.40]	[0.00]	[0.26]	[0.27]	
	F-stat									4.124		
	[p-value]									[0.02]		
	BH 5% c.v.									5.252		
	[BH p-value]									[0.09]		

Notes: The dependent variable is the one-year excess return $\overline{rx}_{t+1}^{(2\to5)} = \frac{1}{4}\sum_{n=2}^{5} rx_{t+1}(n)$. The independent variables are the forward rates: $y_t(1), f_t(2), ..., f_t(5)$, or the five PCs ($PC1$-$PC5$) The regression has an intercept. NW t-stats and NW p-values are computed using Newey-West standard errors with 18 lags. F-stats and the associated p-values report the joint F test for $PC4$ and $PC5$. For both t stats and F stats, we also report the corresponding 5% critical values and p-values of the bootstrap distributions of Bauer and Hamilton (2018).

B.2 Anomalies on the 15th Day of the Month

Figure B.2: **Mid-Month Anomalies**
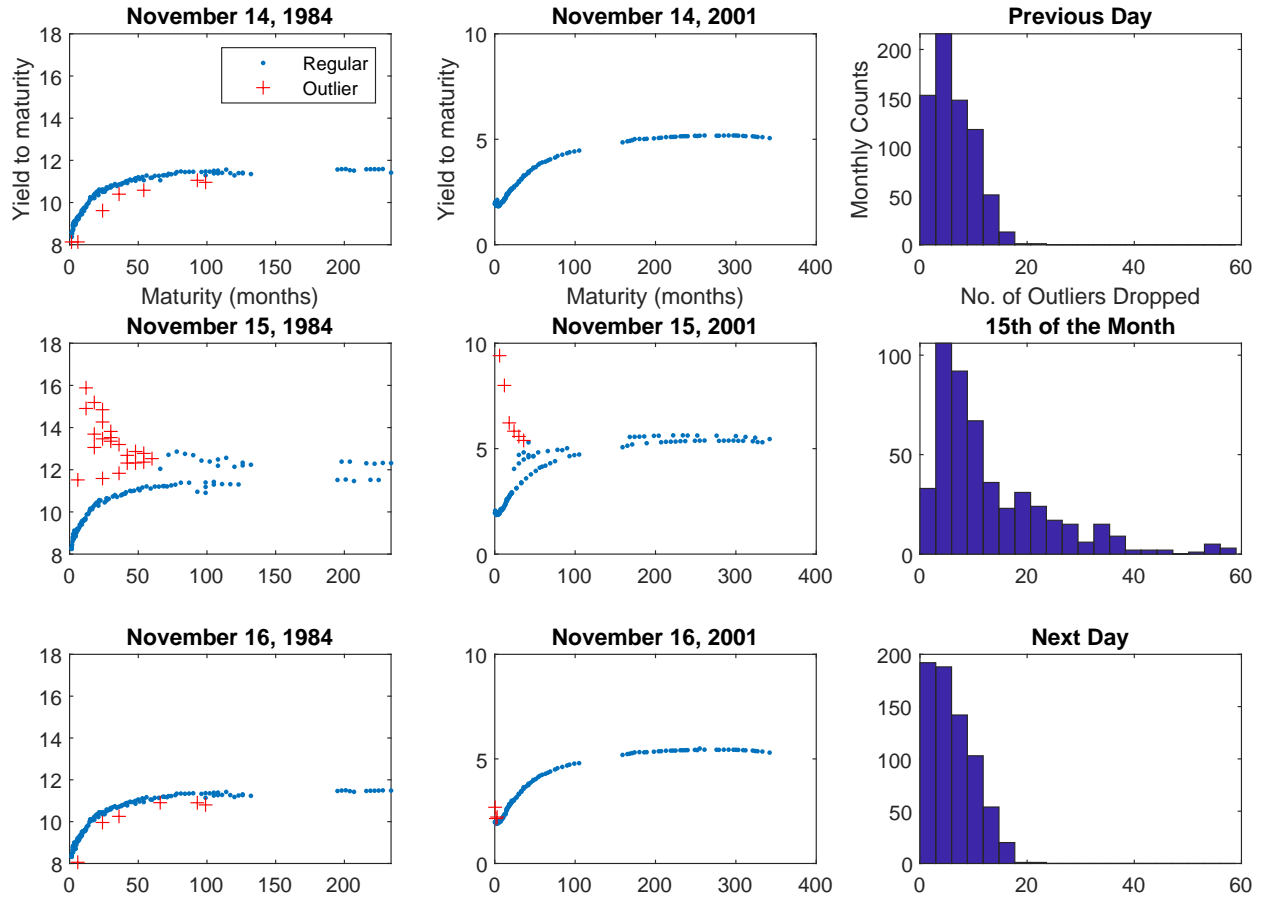
Notes: The first two columns plot the yield to maturity for November 14-16, 1984 (first column) and November 14-16, 2001 (second column). Red +'s mark outliers and blue dots denote bonds we keep. The last column shows the distribution of the number of outliers, and the sample is from June 14, 1961, to December 31, 2019.

B.3 Performance Summary: GSW's Published Parameters

Table B.2: **In-Sample Performance Summary**

	Maturity Bucket									All
	[0,3mth)	[3mth, 1yr)	[1yr, 2yr)	[2yr,5r)	[5yr, 7yr)	[7yr, 10yr)	[10yr, 15yr)	[15yr, 20yr)	[20yr, 30yr]	
LW										
RMSPE	**0.016**	**0.043**	**0.079**	**0.148**	**0.242**	**0.399**	**0.406**	**0.189**	**0.117**	**0.167**
WRMSPE	**0.013**	**0.038**	**0.077**	**0.137**	**0.240**	**0.394**	**0.404**	**0.190**	**0.118**	**0.055**
MAPE	**0.013**	**0.033**	**0.062**	**0.108**	**0.199**	**0.341**	**0.358**	**0.157**	**0.092**	**0.088**
WMAPE	**0.010**	**0.028**	**0.061**	**0.100**	**0.197**	**0.336**	**0.356**	**0.158**	**0.092**	**0.023**
MAPE (Bliss)	**0.006**	**0.016**	**0.032**	**0.063**	**0.139**	**0.261**	**0.260**	**0.111**	**0.059**	**0.055**
WMAPE (Bliss)	**0.005**	**0.014**	**0.030**	**0.057**	**0.138**	**0.256**	**0.258**	**0.112**	**0.059**	**0.012**
MAYE	**0.108**	**0.063**	**0.045**	**0.035**	**0.041**	**0.053**	**0.045**	**0.013**	**0.006**	**0.054**
HR (Bliss)	**0.405**	**0.407**	**0.520**	**0.398**	**0.297**	**0.208**	**0.273**	**0.311**	**0.353**	**0.407**
GSW, Published Parameters										
RMSPE	0.055	0.070	0.103	0.207	0.322	0.594	0.703	0.463	0.511	0.282
WRMSPE	0.046	0.067	0.101	0.194	0.320	0.584	0.696	0.465	0.507	0.099
MAPE	0.050	0.057	0.083	0.154	0.267	0.513	0.617	0.419	0.450	0.153
WMAPE	0.040	0.055	0.082	0.145	0.265	0.503	0.610	0.421	0.446	0.054
MAPE (Bliss)	0.041	0.038	0.048	0.105	0.205	0.426	0.510	0.364	0.410	0.117
WMAPE (Bliss)	0.032	0.039	0.047	0.096	0.203	0.416	0.503	0.366	0.406	0.041
MAYE	0.429	0.124	0.061	0.051	0.054	0.079	0.077	0.033	0.031	0.141
HR (Bliss)	0.183	0.269	0.362	0.262	0.202	0.108	0.128	0.110	0.094	0.243

Notes: We present results for two models: LW (our model) and GSW (using the parameter values published here: https://www.federalreserve.gov/data/nominal-yield-curve.htm). For each maturity bucket (or across all bonds) and for each date, we calculate eight measures of pricing error: root-mean-squared pricing error (RMSPE), duration-weighted root-mean-squared pricing error (WRMSPE), mean absolute pricing error (MAPE), duration-weighted absolute pricing error (WMAPE), mean absolute pricing error adjusted for bid-ask spread (MAPE (Bliss)), duration-weighted absolute pricing error adjusted for bid-ask spread (WMAPE (Bliss)), mean absolute yield error (MAYE), and the hit rate (HR (Bliss)). RMSPE, WRMSPE, MAPE, WMAPE, MAPE (Bliss), and WMAPE (Bliss) are based on a face value of $100. MAYE is based on annualized percentage yield. We report the averaged pricing errors over the full sample from June 1961 to December 2019.
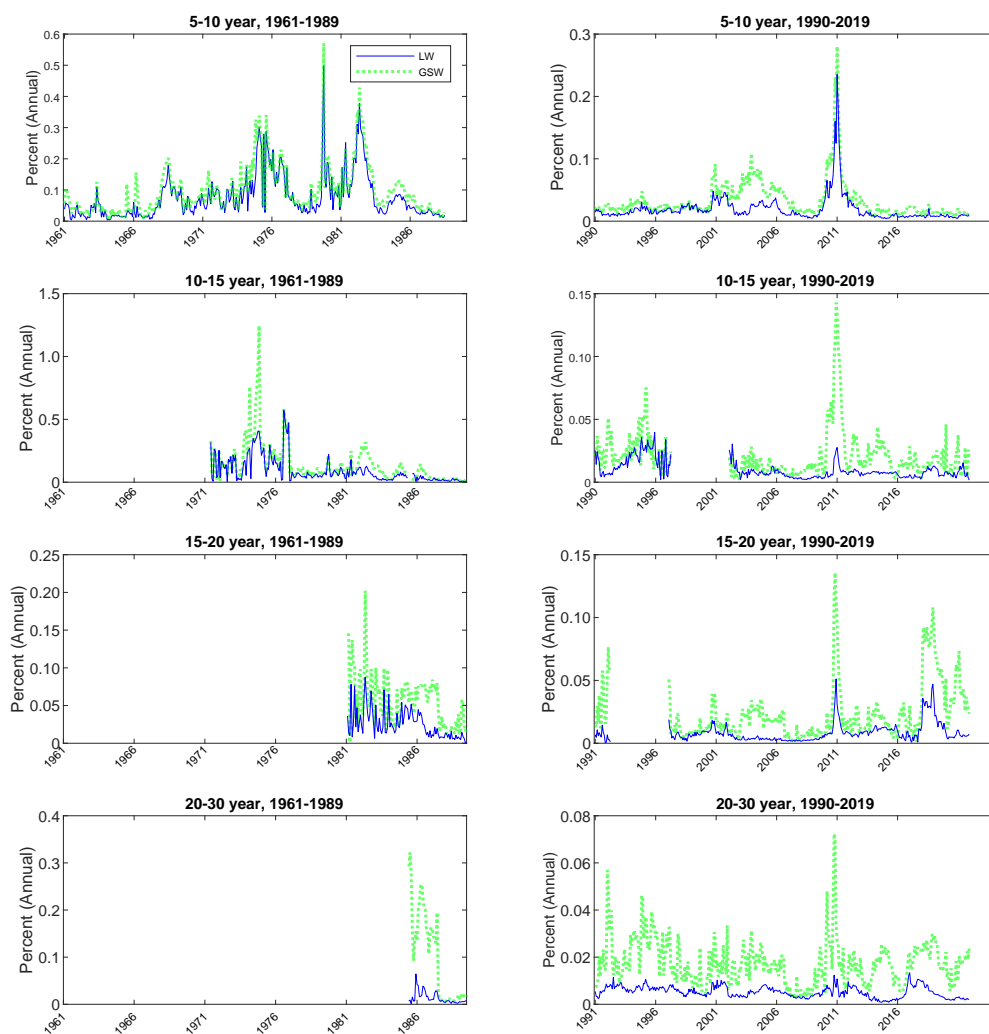
B.4 Time-Series Evidence

Figure B.3: **Time Series of Mean Absolute Error in YTM: The Medium End**
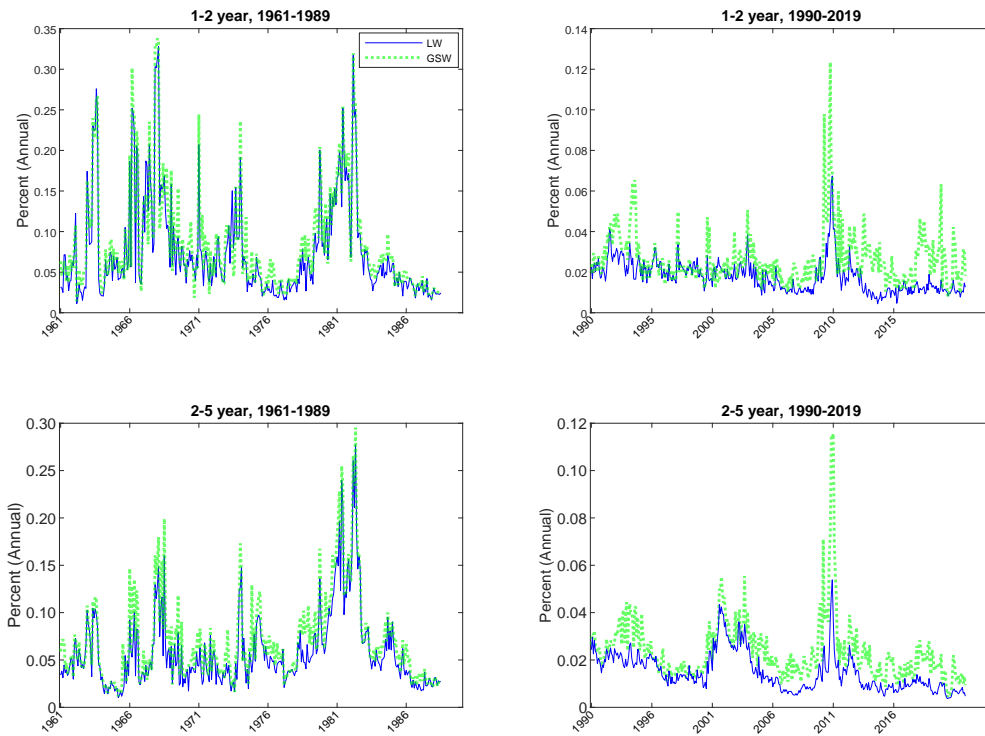
Notes: We plot the mean absolute pricing errors in YTM (i.e., MAYE) for our method and GSW over 1961–1989 (left panels) and 1990–2019 (right panels). We group bonds into two maturity buckets: one- to two-year (top row) and two- to five-year (bottom row).

Figure B.4: **Time Series of Mean Absolute Error in YTM: The Long End**

Notes: We plot the mean absolute pricing errors in YTM (i.e., MAYE) for our method and GSW, over 1961–1989 (left panels) and 1990–2019 (right panels). We group bonds into four maturity buckets: 5–10 year (top row), 10–15 year (second row), 15–20 year (third row), and 20–30 year (bottom row).

B.5 Out-of-Sample Performance

Table B.3: **Out-of-Sample Performance Comparison for Alternative Values of N_0**

				Maturity Bucket						All
	[0,3mth)	[3mth, 1yr)	[1yr, 2yr)	[2yr,5r)	[5yr, 7yr)	[7yr, 10yr)	[10yr, 15yr)	[15yr, 20yr)	[20yr, 30yr]	
Panel A: LW at $N_0 = 4$										
RMSPE	0.016	0.045	0.089	0.175	0.302	0.465	0.605	0.203	0.134	0.209
WRMSPE	0.013	0.039	0.086	0.162	0.300	0.459	0.604	0.205	0.133	0.064
MAPE	0.012	0.033	0.070	0.127	0.250	0.393	0.536	0.163	0.103	0.101
WMAPE	0.010	0.028	0.068	0.117	0.248	0.388	0.533	0.164	0.103	0.024
MAPE (Bliss)	0.006	0.016	0.039	0.080	0.188	0.312	0.435	0.117	0.069	0.068
WMAPE (Bliss)	0.004	0.014	0.037	0.072	0.187	0.307	0.433	0.118	0.068	0.013
MAYE	0.105	0.063	0.052	0.041	0.052	0.061	0.067	0.014	0.007	0.056
HR (Bliss)	0.424	0.407	0.493	0.366	0.251	0.186	0.273	0.297	0.330	0.399
Panel A: LW at $N_0 = 12$										
RMSPE	0.017	0.047	0.091	0.177	0.303	0.485	0.585	0.286	0.195	0.213
WRMSPE	0.014	0.041	0.089	0.164	0.301	0.478	0.583	0.287	0.195	0.065
MAPE	0.014	0.035	0.072	0.127	0.251	0.409	0.527	0.242	0.154	0.107
WMAPE	0.011	0.031	0.070	0.117	0.248	0.404	0.524	0.243	0.154	0.025
MAPE (Bliss)	0.007	0.019	0.039	0.079	0.188	0.329	0.420	0.193	0.117	0.074
WMAPE (Bliss)	0.005	0.015	0.038	0.072	0.186	0.323	0.418	0.195	0.117	0.014
MAYE	0.119	0.068	0.053	0.042	0.051	0.064	0.066	0.019	0.010	0.061
HR (Bliss)	0.375	0.379	0.468	0.357	0.240	0.181	0.183	0.238	0.211	0.365

Notes: We present out-of-sample results for two models: LW at $N_0 = 4$ and LW at $N_0 = 12$. For each maturity bucket (or across all bonds) and for each date, we calculate eight measures of pricing error: root-mean-squared pricing error (RMSPE), duration-weighted root-mean-squared pricing error (WRMSPE), mean absolute pricing error (MAPE), duration-weighted absolute pricing error (WMAPE), mean absolute pricing error adjusted for bid-ask spread (MAPE (Bliss)), duration-weighted absolute pricing error adjusted for bid-ask spread (WMAPE (Bliss)), mean absolute yield error (MAYE), and the hit rate (HR (Bliss)). RMSPE, WRMSPE, MAPE, WMAPE, MAPE (Bliss), and WMAPE (Bliss) are based on a face value of $100. MAYE is based on annualized percentage yield. We report the averaged pricing errors over the full sample from June 1961 to December 2019 at the quarterly frequency.